International Journal of Solids and Structures 288 (2024) 112597

Contents lists available at ScienceDirect

International Journal of Solids and Structures

journal homepage: www.elsevier.com/locate/ijsolstr

Impact induced compression and decompression waves in porous meta-materials modeled using a continuum theory of phase transitions

Konstantinos Garyfallogiannis, Prashant K. Purohit *

Department of Mechanical Engineering and Applied Mechanics, University of Pennsylvania, Philadelphia, PA 19104, USA

ARTICLE INFO

Keywords:
Impact
Shock wave
Fan
Phase transition
Architected materials

ABSTRACT

Porous meta-materials with both regular and random microstructure are of intense research interest today due to their interesting dynamical properties, including but not limited to, their acoustic band structure, shock absorption properties, and fracture toughness. Some of these materials can exist in a rarefied or densified state depending on the state of stress, and recover their original configuration after a cycle of loading and unloading. Often, they exhibit a hysteretic stress–strain response under quasistatic uniaxial compression. As such, many aspects of their mechanical behavior can be captured using a continuum theory of phase transitions. In this work, the dynamical behavior of such materials is explored. It is shown that the impact problem for these materials can result in propagating shocks, phase boundaries, and fans. The impact problems admit multiple solutions for the same set of initial and boundary conditions leading to non-uniqueness. This non-uniqueness can be remedied using a nucleation criterion and kinetic laws, as is known from the continuum theory of phase transitions. The fan solutions which arise in decompressive impact problems have not received much attention in the literature and may be regarded as a novel contribution of this work. The analysis presented here may have applications in the dynamic behavior of a broad class of porous materials including architected truss-like metastructures and random fiber networks.

1. Introduction

Porous meta-materials have emerged as a promising class of materials due to their lightweight, mechanical, thermal, acoustic, and shock absorption properties, amongst others. Cellular (Gibson and Ashby, 1997) and fibrous materials (Picu and Ganghoffer, 2019) encompass the overwhelming majority of porous materials. Their (micro)structure can vary significantly — from architected materials with regular topology, like a honeycomb-type structure (Qi et al., 2021) or TPMS lattices (Al-Ketan and Abu Al-Rub, 2019), to materials with more stochastic or random topology, like foams (Raj, 2011) or carbon nanotube forests (Cao et al., 2005). The characteristic length of the microstructure varies remarkably too, from micrometers, e.g., nanoarchitected carbon materials (Portela et al., 2021) and carbon nanotube forests (Kuzumaki and Mitsuda, 2006), to centimeters, e.g., lattice structures (Schaedler et al., 2011; Ozdemir et al., 2016; Mueller et al., 2019).

The typical equilibrium response of these porous meta-materials under uniaxial compression has three regions in the stress–strain curve: (1) a small region where the material behaves (linear) elastically, followed by (2) a region of softening/stress plateauing corresponding to the onset of instabilities at the structural scale, like intense bending/buckling, plasticity, pore compaction, re-configuration of the structure, and (3) a densified region in which there is self-contact and the collapsed material densifies with stress rising rapidly. In this work, the focus is on materials which do not undergo plastic deformation. As such, the cyclic stress–strain response (in loading and unloading) is repeatable with hysteresis. In other words, the material exhibits the three regions in the stress–strain curve mentioned above, but it comes back to its original configuration when unloaded. Some carbon-nanotube forest materials have this property (Liang et al., 2017b; Park et al., 2020), as do random networks of some biological fibers (Purohit et al., 2011; Kim et al., 2015; Liang et al., 2017a; Garyfallogiannis et al., 2023). These materials have been treated as being capable of phase transitions – from a rarefied phase with straight fibers to a densified phase with buckled fibers – and it has been shown that most aspects of their compression response can be captured using such a model. In particular, this methodology has been applied successfully in the description of static compression of carbon nanotube forests (Liang et al., 2017b). Carbon nanotube materials have intriguing properties and hold potential for many applications (Miao, 2013), e.g., mechanical (Coleman et al., 2006; Peng et al., 2008), thermal (Yu et al., 2005), electrical (Tawfick et al., 2009), optical (Butt et al., 2012). They remain

* Corresponding author.
E-mail address: purohit@seas.upenn.edu (P.K. Purohit).

https://doi.org/10.1016/j.ijsolstr.2023.112597
Received 26 April 2023; Received in revised form 7 October 2023; Accepted 22 November 2023
Available online 30 November 2023

of research interest, so their constitutive behavior, which includes the three representative aforementioned loading stages, is adopted in this work.

Many of these porous materials have excellent shock absorption properties; this is why there is extensive literature on their response under impact loading (Sun and Li, 2018). In the past decades, numerous experimental (just to name a few (Reid and Peng, 1997; Deshpande and Fleck, 2000; Tan et al., 2005a; Jang and Kyriakides, 2009a; Barnes et al., 2014; Ozdemir et al., 2016; Mueller et al., 2019)), theoretical (Herrmann, 1969; Ruzzene et al., 2003; Zheng et al., 2014; Babaee et al., 2015; Gaitanaros and Kyriakides, 2015; Wang et al., 2015), and combined, i.e., experiments and theoretical analysis (Tan et al., 2005a; Jang and Kyriakides, 2009b; Zheng et al., 2012; Kader et al., 2016; Dattelbaum et al., 2020; Khajehtourian and Kochmann, 2020; Portela et al., 2021) efforts have been made to gain insight into the dynamic behavior of porous (meta-)materials. In this work, the problem of dynamic loading of porous meta-materials is treated as a dynamic phase transition problem, in which the pristine material is assumed to be in the rarefied phase, and during compaction, the material transits to the densified phase. The softening/plateauing behavior occurring in the material after the initial elastic loading is associated with the phase transition process. The advantage of modeling the dynamic response as a phase transition problem is the robust continuum mechanics framework developed for these types of problems (Lakes et al., 1993; Knowles, 1999; Abeyaratne and Knowles, 2006; Niemczura and Ravi-Chandar, 2006; Agrawal and Bhattacharya, 2014; Purohit and Bhattacharya, 2002, 2003) and used with success in other dynamic phenomena, like impact induced martensitic transformation (Escobar and Clifton, 1993; Winfree, 1999; Abeyaratne and Knowles, 2000; Niemczura and Ravi-Chandar, 2006), or power generation in ferroelectric materials (Agrawal and Bhattacharya, 2018), and artificial muscle yarns actuation (Zhao and Purohit, 2016). Beyond the dynamic compression problem, the dynamic de-compression problem is also studied in this work, partly because less attention is paid to it in the literature, but mainly because the focus here is on materials that can recover their structure after unloading, so they can be subjected to repeated cycles of dynamic loading/unloading. Furthermore, decompression leads to the propagation of rarefaction waves, or fans, which have not received much attention within the literature on dynamic phase transitions, except in (Winfree, 1999; Knowles, 2002, 2003). Khajehtourian and Kochmann (2020) refer to rarefaction waves which are phase transitions from a densified to a rarefied phase in a multistable architected material, but these are different from the rarefaction waves considered in this work which are also known as rarefaction fans and do not involve phase change.

This work is articulated as follows: in Section 2 a concise description is given of the continuum mechanical theory of dynamic phase transitions utilized in this work. Section 3 provides a short description of the constitutive model adopted, including the double-well stored energy function which is characteristic of phase transforming materials. In Section 4, the initial boundary value problem is defined for the impact induced compression and decompression problem, while in Section 5 the solutions for the compressive impact are presented first, and then are followed by the decompressive impact solutions. In the conclusions, a brief summary is given for how the solutions given here are related to those already discussed in literature and predicted solutions are mentioned, so they may be verified through experiments.

2. Kinematics, balance laws, jump conditions and driving force at a discontinuity

2.1. Description of the problem

Impact problems on a semi-infinite one-dimensional continuum (or bar) are studied in this paper. In the reference state, the continuum occupies the positive x-axis. The continuum is assumed to be semi-infinite to avoid reflection of waves at the right end. Impact problems on finite bars can be solved using a Godunov method which is built using the solutions of impact and Riemann problems (Purohit and Bhattacharya, 2003). These methods can handle reflections and interactions of waves. However, they are beyond the scope of the current work. It is assumed here that the bar is immobile and in mechanical equilibrium under an initial strain γ_i and stress σ_i before the impact occurs. The initial strain γ_i and stress σ_i are usually zero for the compressive impact case, while it is non-zero for the decompressive impact case. The schematic representation of the compressive impact case is depicted in Fig. 1a. The impact takes place at the left boundary of the continuum ($x = 0$) at time $t = 0^+$, whence the left boundary of the continuum is assumed to have the same velocity as the impactor. At later times, a material point occupying the reference position x is displaced to a new position $x + u(x,t)$ with $u(x,t)$ being the longitudinal displacement of that material point at time t.

While the term "impact" implies compressive loading (positive impactor velocities), it is used also for decompressive loading (negative impactor velocities) in this work. Decompressive impact means that the left end of the continuum is pulled leftwards. This happens in the schematic representation of the decompressive impact depicted in Fig. 1b. The exact initial–boundary-value problem for both the compressive and decompressive impact problems is formulated in Section 4.

2.2. Kinematics

A Lagrangian formulation of the problem is adopted in this work, as suggested in Abeyaratne and Knowles (2006), and also used by others (e.g., Zheng et al., 2012; Gaitanaros and Kyriakides, 2015). $u(x,t)$ is the displacement of the particle in the x–direction at time t, and it must be a piecewise continuously differentiable function, i.e., $u(x,t)$ is continuous everywhere and its derivatives are piecewise continuous. The strain $\gamma(x,t)$ and the particle velocity $v(x,t)$ are derived from the displacements $u(x,t)$ as:

$$\gamma(x,t) = u_x(x,t) \qquad \& \qquad v(x,t) = u_t(x,t), \tag{1}$$

where the subscripts denote partial derivatives with respect to position or time. Both $\gamma(x,t)$ and $v(x,t)$ are assumed to be piecewise smooth functions, with possibly a finite number of jump discontinuities. In the Lagrangian description of the problem, kinematic compatibility is expressed through the relation:

$$\gamma_t(x,t) = v_x(x,t). \tag{2}$$

Unique mapping of $x \to x + u(x,t)$ and no material interpenetration is guaranteed by having

$$\gamma(x,t) > -1 \qquad \forall x,t \tag{3}$$

2.3. Balance of linear momentum

Following the Lagrangian description of the problem, the nominal stress $\sigma(x,t)$ experienced by a particle at position x at time t is introduced. Then, the balance of linear momentum is expressed as:

$$\sigma_x(x,t) = \rho v_t(x,t), \tag{4}$$

where ρ is the initial/referential density of the material and $v_t(x,t)$ is the particle acceleration. Assuming that the nominal stress σ is a function of γ alone through a constitutive law, i.e., $\sigma = \sigma(\gamma)$, the chain rule can be used to re-write (4) as the one dimensional wave equation:

$$\sigma'(\gamma(x,t))\,\gamma_x = \rho v_t(x,t). \tag{5}$$

where $\sqrt{\sigma'(\gamma)/\rho}$ is the slope of the characteristic lines in the x–t plane.

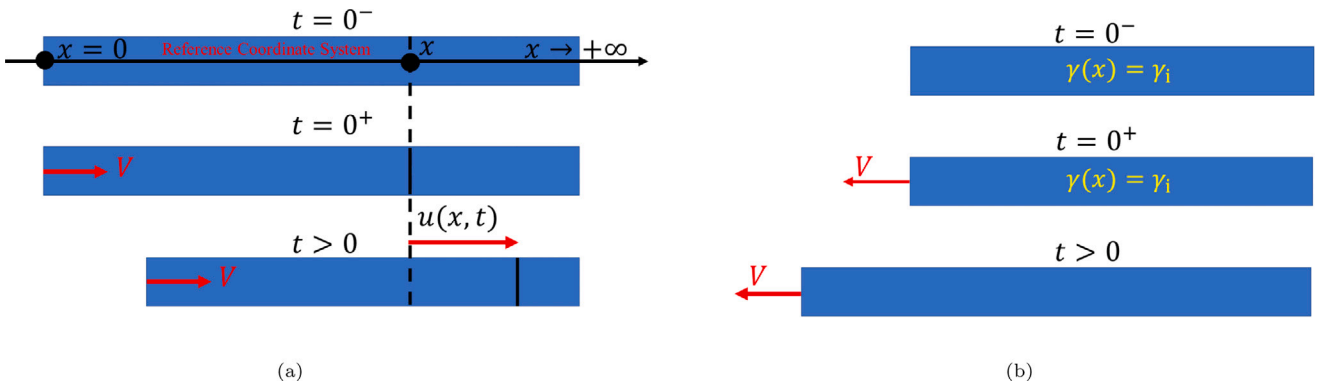

Fig. 1. Schematic representations of different instants of a bar subject to (a) a compressive, and (b) a decompressive impact. The rectangles represent the bar in the current configuration. The black line in the top left rectangle is the one dimensional reference coordinate system superimposed on the stress free bar before impact.

2.4. Jump conditions

The problem of interest includes discontinuities which can be shock waves and phase transition fronts in the medium, as will become clearer soon. Both shock waves and phase transition fronts are surfaces at which quantities like strain, stress, particle velocity, etc. may suffer finite jumps. The degree of smoothness assumed here is enough to permit such jumps at a finite number of places, while the fields remain smooth everywhere else in the medium. In the simpler one-dimensional theory presented here, these singular surfaces are replaced by singular points, which travel through the medium, i.e. they are not stationary. One such singular point is at the referential location $x = s(t)$ at time t, and traverses the continuum with a Lagrangian (or referential) velocity $\dot{s}$.

For an arbitrary smooth–enough function $g(x,t)$ the jump at discontinuity $s(t)$ is defined as

$$[\![g]\!] = g(s^+,t) - g(s^-,t), \tag{6}$$

which is the difference between the values of $g(x,t)$ as one approaches the discontinuity from the plus (right) and minus (left) sides. The one-dimensional Lagrangian jump conditions which arise from the continuity of the motion $u(x,t)$ of the particle and the balance of linear momentum (Gurtin et al., 2010) are:

1. Kinematic jump condition:

$$[\![v]\!] = -\dot{s}[\![\gamma]\!]. \tag{7}$$

2. Linear momentum jump condition:

$$[\![\sigma]\!] = -\rho\dot{s}[\![v]\!]. \tag{8}$$

The Lagrangian velocity $\dot{s}$ with which the discontinuity traverses the medium is derived by replacing (7) into (8):

$$\dot{s} = \sqrt{\frac{1}{\rho}\frac{[\![\sigma]\!]}{[\![\gamma]\!]}}, \quad \text{or,} \quad \rho\dot{s}^2 = \frac{\sigma^+ - \sigma^-}{\gamma^+ - \gamma^-}. \tag{9}$$

Relation (9) attributes a geometric interpretation to the discontinuity velocity $\dot{s}$. That is, $\rho\dot{s}^2$ is the slope of the chord connecting the stress–strain states, before (i.e., (γ^+,σ^+)) and after (i.e., (γ^-,σ^-)) the discontinuity in the stress–strain curve $\sigma(\gamma)$.

2.5. Driving force acting on a discontinuity

The next step is to perform a balance of mechanical power on a portion of the one-dimensional continuum in the interval (x_1,x_2) in the reference configuration such that $x_1 < s(t) < x_2$. If the rate of work on the boundaries of the continuum (per unit reference volume) is $\dot{W}(t)$ and the rate of energy stored in mechanical deformations (per unit reference volume) is $\dot{U}(t)$, then the dissipated energy rate $\dot{D}(t)$ (per unit reference volume) is given by the difference between these two rates. This statement can be localized to the discontinuity to express the dissipation rate as a product of a driving force $f(t)$ and speed $\dot{s}(t)$ as (Purohit and Bhattacharya, 2003):

$$\dot{D}(t) = \dot{W}(t) - \dot{U}(t) = f(t)\dot{s}(t). \tag{10}$$

Thus, the propagation of discontinuities dissipates energy. On every discontinuity moving with a Lagrangian velocity $\dot{s}(t)$ a driving force $f(t) = f(\gamma^-,\gamma^+)$ is exerted. The expression for f can be computed from the balance of mechanical power after combining it with the balance of linear momentum. The result is Abeyaratne and Knowles (2006):

$$\begin{aligned} f(t) &= [\![U(\gamma)]\!] - \frac{1}{2}\left[\sigma(\gamma^+) + \sigma(\gamma^-)\right][\![\gamma]\!] \\ &= \int_{\gamma^-}^{\gamma^+} \sigma(\gamma)d\gamma - \frac{1}{2}\left[\sigma(\gamma^+) + \sigma(\gamma^-)\right](\gamma^+ - \gamma^-) \end{aligned} \tag{11}$$

From (11) the driving force is geometrically interpreted as the signed difference between the area of the stress–strain curve from γ^- to γ^+ and the trapezoid made from the points $(\gamma^-,0)$, $(\gamma^+,0)$, (γ^+,σ^+) and (γ^-,σ^-). The geometric interpretations of the driving force in (11) and the discontinuity velocity in (9) are presented in Figs. 2a and b for the compressive and decompressive impact, respectively. These representations of the problem provide a graphic tool to understand the nature of the solution before the initial boundary value problem (IBVP) is even solved, as is shown later in this work.

Here the driving force can be perceived as a thermodynamic force driving the process of phase transition. The notion of driving force goes back to Eshelby (1951) who wrote down a generalized force on a singularity, which laid the foundation for Rice (1968) to interpret that generalized force in the context of fracture mechanics as the energy release rate at crack advancement. Abeyaratne and Knowles (1990) studied the driving force (traction) on a surface of strain discontinuity for a thermomechanical problem. They showed that non-uniqueness in the solution of Riemann and impact problems involving martensitic phase transitions can be removed by invoking kinetic relations that relate the speed $\dot{s}$ to the driving force $f(\gamma^-,\gamma^+)$ acting on the discontinuity.

Relation (10) poses important restrictions on admissible solutions to initial boundary value problems involving moving discontinuities. From the second law of thermodynamics, the dissipation rate should be non-negative:

$$\dot{D}(t) = f(t)\dot{s}(t) \geq 0. \tag{12}$$

For both compressive and decompressive impact, the discontinuities propagate from left to right (see Fig. 1), meaning it is always true that $\dot{s}(t) \geq 0$. Consequently, all admissible solutions with the propagation of discontinuities in both compressive and decompressive impact problems must satisfy the requirement of $f(t) \geq 0$. For the special case of discontinuities propagating in linear media (sonic waves), the driving force vanishes, i.e., the propagation is dissipation–free.

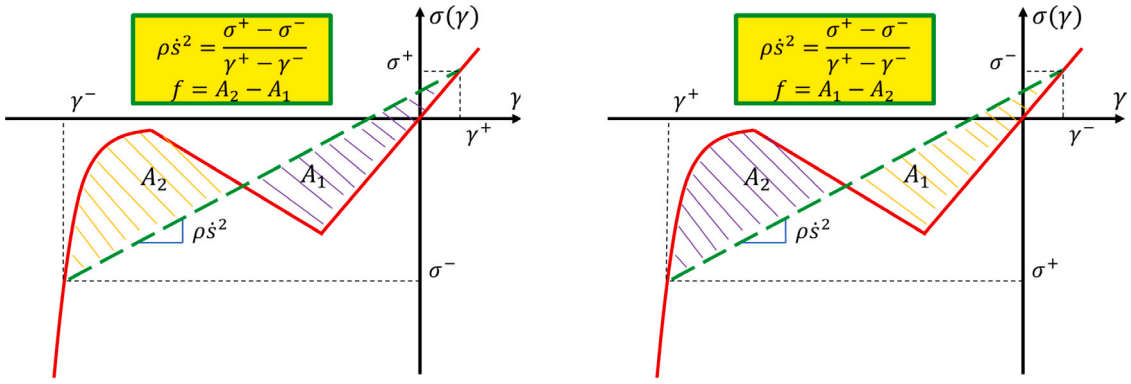

(a) Compressive Impact (b) Decompressive Impact

Fig. 2. Geometric interpretation of the discontinuity velocity in (9) and the driving force in (11) for (a) the compressive, and (b) the decompressive impact.

3. Constitutive model

The continuum constitutive model is one-dimensional, i.e. depends only on the strain γ. Denoting with $U(\gamma)$ the stored energy density per unit reference volume associated with the strain γ, the nominal stress $\sigma(\gamma)$ is given by:

$$\sigma(\gamma) = \frac{dU}{d\gamma}. \tag{13}$$

The stress as a function of the strain γ is chosen to be that of a carbon nanotube forest material (Liang et al., 2017b) as described in (14), as these materials are of interest in applications. This work is confined mostly to compressive strains, and the stress–strain curve in (14) has the qualitative behavior observed in porous materials which can recover their original configuration upon unloading. More specifically, the stress–strain relation incorporates the description of a linear phase ((14)a), which is usually called rarefied phase, the unstable phase with negative slope of the stress–strain curve ((14)b), and a non-linear phase ((14)c), which is usually called densified. For plastic deformations under impact loading other constitutive relations are also utilized, which have the same qualitative behavior as the one suggested here, i.e., linear phase, followed by a hardening crushed phase (e.g., Deshpande and Fleck, 2000; Tan et al., 2005a,b; Kader et al., 2016).

$$\sigma(\gamma) = \frac{dU}{d\gamma} = \begin{cases} E\gamma & \gamma \geq -\gamma_m, \\ \alpha_1\gamma + \alpha_2 & -\gamma_M \leq \gamma \leq -\gamma_m, \\ \dfrac{A-B}{(1+\gamma)^3} + B & -1 < \gamma \leq -\gamma_M. \end{cases} \tag{14}$$

The linear/rarefied phase is the unperturbed/pristine phase of the material and is applicable for strains $\gamma \geq -\gamma_m$. It is assumed that the linear region of the stress–strain response is valid also for the tensile strains. Under compression, the buckling of the carbon nanotube forests results in an unstable region over the range $-\gamma_M \leq \gamma \leq -\gamma_m$. In absence of knowledge of its exact form and following previous works (Abeyaratne and Knowles, 2000), it is assumed to be linear with a negative slope. The negative slope, or softening regime, which is associated with bending instability is observed in quasi-static compression of honeycomb structures (Xiong et al., 2016; Wei et al., 2019) or tension of multi-stable architectured materials (Jin et al., 2020), programmable buckling of micro-lattices (Frenzel et al., 2016), dynamic compression of aluminum foams (Tan et al., 2005a), quasi-static (Lakes et al., 1993; Schaedler et al., 2011; Al-Ketan and Abu Al-Rub, 2019) and dynamic (Smith et al., 2011; Ozdemir et al., 2016) compression of lattice structures (Schaedler et al., 2011), and carbon nanotubes (Kuzumaki and Mitsuda, 2006; Shima, 2011). These instabilities corresponding to negative slope are also seen in the compression of carbon nanotube foams (Pathak et al., 2012; Hutchens et al., 2012). For compressive strains $-1 < \gamma \leq -\gamma_M$, the non-linear response is given by the hyperbola in ((14)c), which asymptotes at $\gamma = -1$. As $\gamma \to -1$, the material gets highly crushed and compressed. The stress–strain law in (14) is depicted schematically in Fig. 3a. Various constants entering this constitutive law are given in Table 1 and correspond to three different materials. In the above E, α_1, α_2, A and B are constants that may be fitted to experimental data. Utilizing (13), the stored energy density $U(\gamma)$, corresponding to the stress in (14), is given in (15) and is depicted in Fig. 3b:

$$U(\gamma) = \begin{cases} \dfrac{E}{2}\gamma^2 + C_1 & \gamma \geq -\gamma_m, \\ \dfrac{\alpha_1}{2}\gamma^2 + \alpha_2\gamma + C_2 & -\gamma_M \leq \gamma \leq -\gamma_m, \\ -\dfrac{A-B}{2(1+\gamma)^2} + B\gamma + C_3 & -1 < \gamma \leq -\gamma_M. \end{cases} \tag{15}$$

The material parameters in (15) are chosen in the following way: E, A, and B are taken from actual experiments (Liang et al., 2017b). The initial density ρ is assigned a value that is representative of these porous materials; numerical experimentation showed that the results depend weakly on the value of ρ. The strain $-\gamma_M$ at which the densified phase begins is of greater importance for the material response than the lower strain of the rarefied phase $-\gamma_m$. Hence, $-\gamma_m$ is taken to be a small enough strain, while there is some freedom in picking $-\gamma_M$ because the experiments cannot provide information directly about its value. α_1 and α_2 are taken such that the unstable linear response satisfies the continuity of $\sigma(\gamma)$ at the transformation strains, i.e., $\sigma(-\gamma_m^+) = \sigma(-\gamma_m^-)$ and $\sigma(-\gamma_M^+) = \sigma(-\gamma_M^-)$. C_1 is selected such that for a pristine material for $\gamma = 0$ the energy in (15)a vanishes, i.e., $C_1 = 0$. C_2 and C_3 are selected such that the energy is continuous at the transformation strains, i.e., $U(-\gamma_m^+) = U(-\gamma_m^-)$ and $U(-\gamma_M^+) = U(-\gamma_M^-)$.

Table 1
Material parameters for the different materials used.
Source: Taken from Liang et al. (2017b).

Material	E [MPa]	A [MPa]	B [MPa]	ρ [kg/m^3]	γ_m	γ_M
1	6	0.66	0.67	2000	0.05	0.76
2	20	1.36	1.37	2000	0.05	0.82
3	6	0.66	0.67	2000	0.05	0.70

4. Initial boundary value problem

The governing equations of the problem are laid out explicitly in Section 2. In order to fully define the initial boundary value problem a set of boundary and initial conditions need to be prescribed. These conditions have been outlined in Section 2.1 and in Fig. 1, but are formally presented here.

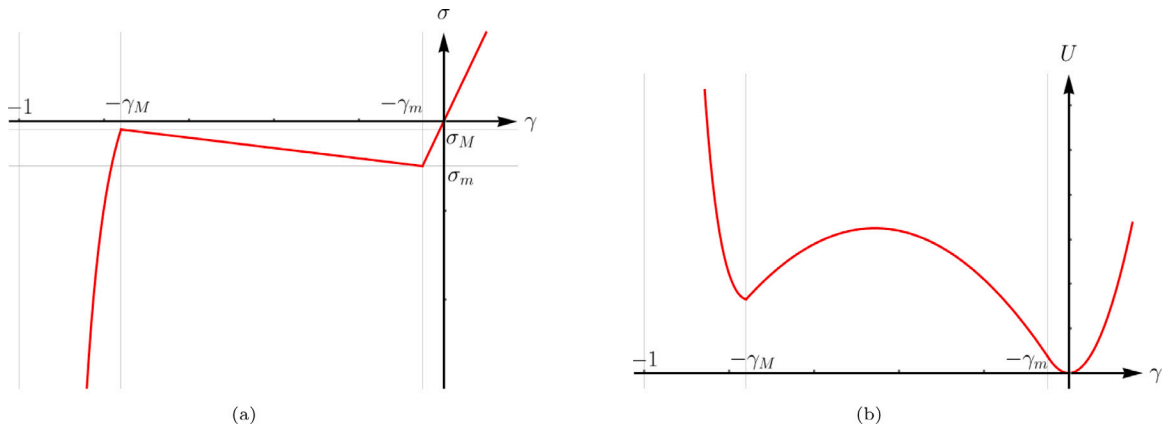

Fig. 3. Schematic representation of the one-dimensional (a) continuum stress–strain constitutive relation in (14), and (b) stored energy density in (15).

4.1. Initial conditions

The continuum is assumed to exist at a pre-strain of γ_{i} prior to the impact:

$$\gamma(x, t \leq 0^{-}) = \gamma_{\mathrm{i}} \quad \text{for } x \geq 0, \tag{16}$$

and at a stress $\sigma_{\mathrm{i}} = \sigma(\gamma_{\mathrm{i}})$. For a pristine specimen, which underwent no loading in advance, it is true that $\gamma_{\mathrm{i}} = 0$. A non-zero pre-strain arises from the prior loading of the material. For example, an initial compressive impact could compress the material at a strain γ_{i}, and subsequently, the loading is reversed (assuming that the dynamics of the original impact have fully damped out).

The continuum is also assumed to be immobile at the time of the impact with its left end being located at $x = 0$.

$$v(x, t \leq 0^{-}) = 0 \quad \text{for } x \geq 0. \tag{17}$$

A non-zero velocity of the continuum prior to impact is not of high interest for actual experimental configurations. The only difference in the analysis presented would be that it makes the impactor velocity look greater (opposite directions) or smaller (same directions). But the solutions presented include all the possible impactor velocities since $V \in (-\infty, +\infty)$, the case of non-zero initial velocity is included implicitly.

4.2. Boundary conditions

The boundary condition applied is that after impact the left end of the continuum moves at the impactor velocity.

$$v(0, t) = \pm V \quad \text{for } t \geq 0^{+}. \tag{18}$$

The (+) sign corresponds to compressive impact, while the (−) sign to decompressive impact. To summarize, the exact initial boundary value problem is defined by the kinematic compatibility relation (2), the conservation of linear momentum (4), the kinematic jump condition (7), the momentum jump condition (8), the constitutive law (14), and the dissipation inequality (12) if a discontinuity is present, the initial conditions on the strain (16) and the velocity (17) accompanied with the boundary condition (18) of impact.

5. Results

For time $t < 0$ the equations of motion are satisfied trivially because the initial conditions correspond to constant strain and zero particle velocity everywhere. The boundary condition changes discontinuously at $t = 0^{+}$ to a non-zero particle velocity at $x = 0$; this discontinuity at the boundary will propagate into the bar $x > 0$ because the equation of motion is a wave equation. As such, the solutions of interest are those in which $u(x, t)$ is continuous for $x \geq 0$ and $t \geq 0$, with possibly discontinuous particle velocities $v(x, t)$ and strains $\gamma(x, t)$. The simplest solutions with discontinuities in particle velocity and strain are those in which these quantities are piece-wise constant for $x \geq 0$, $t \geq 0$. For such solutions the equation of motion is trivially satisfied at all points in the x–t plane except at discontinuities. The jumps in the strain, particle velocity and stress at these discontinuities must satisfy the kinematic jump condition in (7) and momentum jump condition in (8). The solution to the compressive impact problem with the constitutive model in (14) admits two types of discontinuities — shock waves and phase transition fronts. For a shock wave the strains and stresses on both sides of a discontinuity are on the same branch of the stress–strain curve, and for a phase transition front they are on different branches. A shock wave or phase transition front is considered admissible only if its dissipation rate $\dot{D}$ is non-negative. Several x–t planes with piecewise constant strains and particle velocities could be constructed to satisfy a given set of boundary and initial conditions as discussed at length in Abeyaratne and Knowles (2006) and references therein, and shown below. Therefore, extra conditions must be imposed on the initial–boundary value problem to pick a unique solution corresponding to a particular x–t plane.

For the decompression problem, a rarefaction wave (fan) is also an admissible solution when the material is highly strained, in addition to the previously stated solutions with piece-wise constant strain and particle velocity fields. A fan is a continuous solution for which the driving force vanishes. Solutions involving fans are not discussed at length in Abeyaratne and Knowles (2006), but they can be found in the literature (see Knowles, 2002, for example). Solutions involving fans are discussed in the context of phase changing meta-materials in the following.

5.1. Compressive impact

For a compressive impact the initial strain γ_{i} can either be $\gamma_{\mathrm{i}} \leq -\gamma_M$ or $\gamma_{\mathrm{i}} \geq -\gamma_m$. The material cannot exhibit strain in the unstable region $-\gamma_M < \gamma_{\mathrm{i}} < -\gamma_M$. For the initial boundary value problem there is exactly one solution for $\gamma_{\mathrm{i}} \leq -\gamma_M$ and three possible solutions for $\gamma_{\mathrm{i}} \geq -\gamma_m$, and each one has its own x–t plane. For $\gamma_{\mathrm{i}} \geq -\gamma_m$, two out of three possible solutions involve propagating phase boundaries. This non-uniqueness is well-known; a unique solution is selected only if a kinetic relation and a nucleation criterion are specified for the phase boundary. The kinetic relation is of the form $\dot{s} = \phi(f)$ and the nucleation criterion can be for example that f needs to be greater than a lower bound value for an interface to nucleate (Abeyaratne and Knowles, 2006; Knowles, 1999). A specific example showing how a nucleation criterion and kinetic relation lead to a unique solution is described in the Appendix. For the case with initial strain $\gamma_{\mathrm{i}} \geq -\gamma_m$, i.e., the prestrained material is still in the rarefied phase, it is assumed

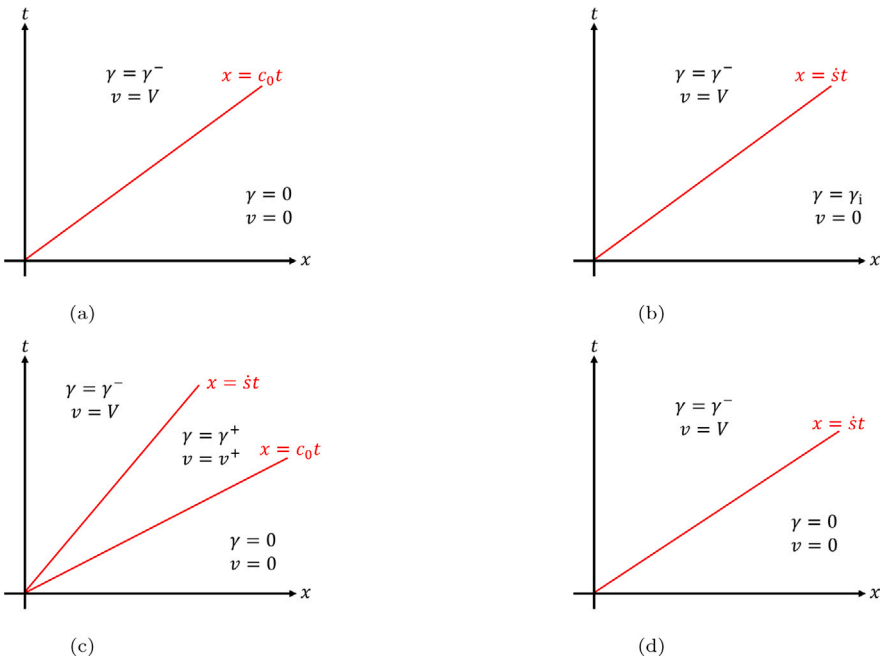

Fig. 4. The possible x–t planes of the compressive impact problem for (a) a sonic wave propagating in the unstrained rarefied phase (b) a shock wave propagating in the pre-strained ($\gamma_i \leq -\gamma_M$) densified phase, (c) a sonic wave propagating in the unstrained rarefied phase followed by a phase transition front, and (d) the overdriven transition front.

that $\gamma_i = 0$. This corresponds to a pristine unloaded material and is of practical interest. However, the analysis presented below for $\gamma_i \geq -\gamma_m$ holds for any $-\gamma_m \leq \gamma_i \neq 0$. Similarly to the way it is done in this work, jump conditions are utilized by Zheng et al. (2012, 2014), and Gaitanaros and Kyriakides (2015) in order to describe the observed behavior from experiments and finite element simulations.

Knowing that no more than two discontinuities can exist in the medium (Abeyaratne and Knowles, 2006), the four cases considered for the compression problem are:

1. A sonic wave propagates in the unstrained rarefied phase, with the x–t plane as shown in Fig. 4a.
2. A shock wave propagates in the pre-strained densified phase ($\gamma_i \leq -\gamma_M$), with the x–t plane as shown in Fig. 4b.
3. A sonic wave propagates in the unstrained rarefied phase followed by a phase transition front transforming material from the rarefied to the densified phase, with the x–t plane as shown in Fig. 4c.
4. A phase transition front propagates supersonically into the unstrained rarefied phase transforming material to the densified phase, with the x–t plane as shown in Fig. 4d. This is called the overdriven case (Abeyaratne and Knowles, 2006).

5.1.1. Sonic wave in the unstrained rarefied phase

The first case appears for weak impactor velocities and includes only one propagating shock (sonic) wave in the unstrained medium, such that the material ahead and behind the wave is in the rarefied (linear) phase, as seen in Fig. 4a. The resulting stress–strain curves are linear, and this case is qualitatively similar to the so-called "Quasi-static Mode" of deformation observed in slow impact loading of cellular materials in Zheng et al. (2012) or "Weak Shock" in slow impact of aluminum foams (Gaitanaros and Kyriakides, 2014). Similar linear stress–strain profiles are observed in Fig. 7 in Zheng et al. (2012), and Figs. 18b and 20 in Gaitanaros and Kyriakides (2014). For a linear material with Young's modulus E, the dissipated energy vanishes, and the sonic wave propagation velocity is derived from (9):

$$c_0 = \sqrt{\left.\frac{d\sigma/d\gamma}{\rho}\right|_{\gamma=0}} = \sqrt{\frac{E}{\rho}}, \tag{19}$$

The impactor velocity V is the parameter of the problem and the only unknown is γ^-. From the kinematic jump condition (7):

$$[\![v]\!] = -\dot{s}[\![\gamma]\!] \Rightarrow V = -c_0\gamma^-. \tag{20}$$

Hence, the strain and particle velocities profiles satisfying the initial boundary value problem are piecewise constant and they are:

$$\gamma(x,t) = \begin{cases} -V/c_0 & \text{for} \quad 0 < x < c_0 t \\ 0 & \text{for} \quad x > c_0 t \end{cases}, v(x,t) = \begin{cases} V & \text{for} \quad 0 < x < c_0 t \\ 0 & \text{for} \quad x > c_0 t \end{cases} \tag{21}$$

This solution will appear for all impact velocities smaller than an upper bound which can be obtained by insisting that $\gamma \leq -\gamma_m$. This means that the impactor velocity V in (21) must satisfy the condition: $V \leq c_0\gamma_m$. The stress profile with the jump in the bar for two different instants for an impactor velocity $V_0 = 2$ m/s ($< c_0\gamma_m$) is plotted in Fig. 6a.

5.1.2. Shock wave in the prestrained densified phase

Similar to the propagation of a shock wave in the unstrained rarefied phase, is the propagation of a shock wave in the prestrained densified phase during compression. In this case, though, the material exists initially at a strain $\gamma_i \leq -\gamma_M$ and stress $\sigma(\gamma_i) = \sigma_i$. Again there is no phase transition and the shock wave transverses the medium from the left (behind the wave region) to the right (ahead of the wave region), as seen in Fig. 4b. The impactor velocity V and the initial strain γ_i are parameters of the problem and the unknowns are the strain after the shock wave γ^- and its propagation velocity $\dot{s}$. The kinematic jump condition (7) gives:

$$[\![v]\!] = -\dot{s}[\![\gamma]\!] \Rightarrow \dot{s} = \frac{V}{\gamma_i - \gamma^-}, \tag{22}$$

which results in the following piecewise constant strains and particle velocities profiles satisfying the initial boundary value problem:

$$\gamma(x,t) = \begin{cases} \gamma_i - V/\dot{s} & \text{for} \quad 0 < x < \dot{s}t \\ \gamma_i & \text{for} \quad x > \dot{s}t \end{cases}, v(x,t) = \begin{cases} V & \text{for} \quad 0 < x < \dot{s}t \\ 0 & \text{for} \quad x > \dot{s}t \end{cases} \tag{23}$$

Replacing (22) in the stress jump condition (8):

$$[\![\sigma]\!] = -\rho\dot{s}[\![v]\!] \Rightarrow \sigma_i - \sigma(\gamma^-) = \rho\frac{V^2}{\gamma_i - \gamma^-}, \tag{24}$$

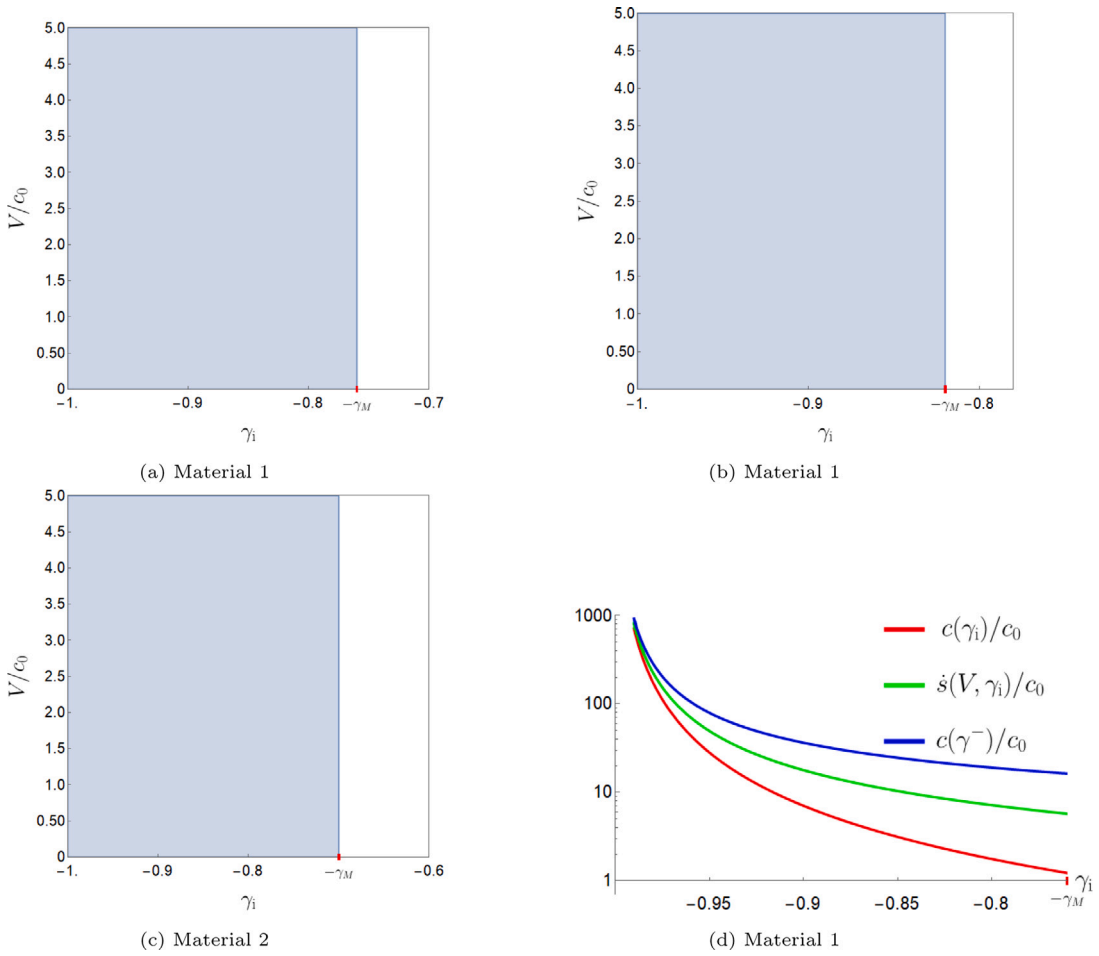

Fig. 5. (a) - (c) Admissible solutions where the driving force is positive $f \geq 0$ and $-1 < \gamma^- \leq \gamma_i$ for (a) Material 1, (b) Material 2, and (c) Material 3. Note that any combination of initial strain $-1 < \gamma_i \leq -\gamma_M$ and impactor velocity V provides an admissible solution. (d) Shock wave velocity $\dot{s}$ for Material 1 impacted with $V = c_0$ compared with sonic wave velocities.

which results in a quartic equation for γ^-, which is too lengthy to write here. Only one of the four roots provides admissible solutions in terms of strains and driving force, i.e., $-1 < \gamma^- \leq \gamma_i$ and $f \geq 0$. Unlike the shock wave propagation in the linear rarefied phase, in the densified phase the driving force, and the dissipated energy, are non-zero and always positive. Figs. 5a-c present the region of the V–γ_i plane where admissible solutions exist for the three different materials in Table 1. Note that for every combination of an initial strain γ_i and impactor velocity V, there is always a solution to the problem. Fig. 5d shows that the propagation velocity $\dot{s}$ of the shock wave in the densified non-linear phase always lies between the sonic wave velocities corresponding to strains γ_i and γ^-:

$$c_i = c(\gamma_i) = \sqrt{\frac{d\sigma/d\gamma}{\rho}}\bigg|_{\gamma=\gamma_i}, \quad \text{and} \quad c^- = c(\gamma^-) = \sqrt{\frac{d\sigma/d\gamma}{\rho}}\bigg|_{\gamma=\gamma^-}. \tag{25}$$

The impactor velocity in Fig. 5d is chosen to be $V = c_0$, but the trend is the same for any V and all materials in Table 1. Also, it is interesting to note the fast shock wave velocities $\dot{s}$ (logarithmic vertical axis normalized by $V = c_0$) arising in the problem, e.g. for $\gamma_i = -0.9$, $\dot{s} \approx 20c_0$.

5.1.3. A sonic wave followed by a phase transition front

A sonic wave can propagate in the unstrained rarefied phase, followed by a phase transition front converting the material from the rarefied to the densified phase, as seen in Fig. 4c. Fig. 2a illustrates geometrically the driving force and the discontinuity velocity $\dot{s}$. The phase transition front propagates with a subsonic velocity, i.e. $\dot{s} \leq c_0$. In the one-dimensional continuum, three distinct regions are observed at any moment. The first region is already traversed by the sonic wave and the phase transition front ($0 < x < \dot{s}t$), and it lies in the densified phase. All the material points move with velocity V and the strain is γ^-. The second region is traversed only by the shock wave ($\dot{s}t < x < c_0t$) and lies in the rarefied phase. The solution for this regime has the same structure as in (21) for $0 < x < c_0t$. Lastly, there is the unperturbed/unstrained material ($x > c_0t$).

This mode of deformation appears for intermediate impactor velocities. It is analogous to the so-called "Transitional Mode" observed for foams in Zheng et al. (2012) (if one recognizes that $c_0 \to +\infty$ in their case because the unperturbed material is modeled as rigid and not linearly elastic) or two-dimensional honeycombs in Zheng et al. (2005). Elastic "precursor waves" before the compaction waves are met in experiments in foams too (Lopatnikov et al., 2004; Petel et al., 2014; Kader et al., 2016). This mode of deformation is also observed in the dynamic compression of engineered lattice materials (Hawreliak et al., 2016) where the phase transition wave is called the "compaction wave". In mathematical form:

$$\gamma(x,t) = \begin{cases} \gamma^- & \text{for} \quad 0 < x < \dot{s}t \\ \gamma^+ & \text{for} \quad \dot{s}t < x < c_0t \\ 0 & \text{for} \quad x > c_0t \end{cases}, v(x,t) = \begin{cases} V & \text{for} \quad 0 < x < \dot{s}t \\ v^+ & \text{for} \quad \dot{s}t < x < c_0t \\ 0 & \text{for} \quad x > c_0t \end{cases} \tag{26}$$

The unknowns in (26) are γ^+, γ^-, v^+, while the impactor velocity V, as well as the phase transition front speed $\dot{s}$ are parameters of the problem. The structure of the solution in Fig. 4c and (26) is the same as the one obtained for phase-transitioning dissipative multistable

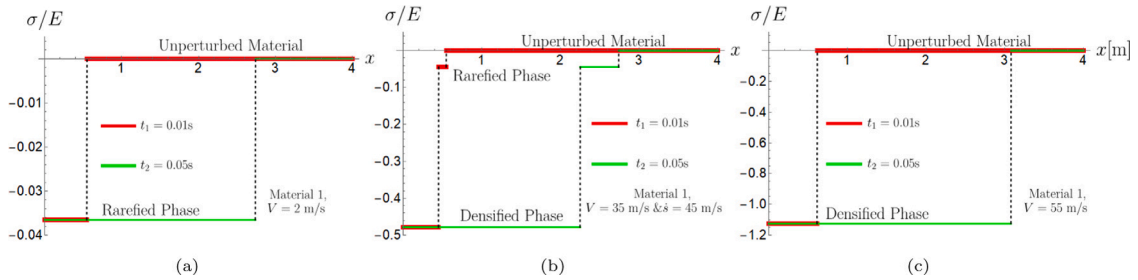

Fig. 6. Stress profiles in the bar for the compressive impact for Material 1. (a) Sonic wave, (b) sonic wave followed by phase transition front, and (c) overdriven phase transition.

metamaterials in Khajehtourian and Kochmann (2020). For the sonic wave discontinuity, the kinematic jump condition in (7) results in:

$$[\![v]\!] = -\dot{s}[\![\gamma]\!] \Rightarrow v^+ = -c_0\gamma^+. \tag{27}$$

Utilizing the velocity and stress jump conditions in (7) and (8) for the phase transition discontinuity, respectively, γ^+ and γ^- are found. The solutions are parametric with respect to the impactor velocity V and the phase transition velocity $\dot{s}$. Beginning with the jump condition in (7), γ^+ is:

$$[\![v]\!] = -\dot{s}[\![\gamma]\!] \Rightarrow \gamma^+ = \frac{V + \dot{s}\gamma^-}{\dot{s} - c_0}. \tag{28}$$

Replacing (28) in (8), simplifying and rearranging terms leads to the following quartic equation for γ^-:

$$c\rho\dot{s}(\gamma^-)^4 + \{B + \rho[3c\dot{s} + (c+\dot{s})V]\}(\gamma^-)^3 + 3\{B + \rho[\dot{s}V + c(V+\dot{s})]\}(\gamma^-)^2 + \{3B + \rho[c\dot{s} + 3V(c+\dot{s})]\}\gamma^- + (c+\dot{s})\rho V + A = 0. \tag{29}$$

Eq. (29) is solved in closed form using the computational software Mathematica. Note that $\dot{s}$ is a parameter in (29). In other words, one can pick $\dot{s}$ freely and each $\dot{s}$ corresponds to a different solution of the impact problem satisfying all balance laws and jump conditions. Thus, we have massive non uniqueness in the possible solutions. To pick a particular $\dot{s}$ and get rid of the non-uniqueness a kinetic relation must be specified. Often, this kinetic relation is of the form $\dot{s} = \phi(f)$ where f is the driving force on the phase transition front. To satisfy the dissipation inequality the kinetic law must satisfy $f\dot{s} = f\phi(f) \geq 0$ for all values of f. A simple choice of kinetic relation and how this leads to a unique value of $\dot{s}$ is discussed in the Appendix. Here we let $\dot{s}$ remain a parameter because our interest is in mapping out the space of possible solutions. The resulting expressions/roots for γ^- are lengthy and are not reproduced here. γ^+ can then be calculated from γ^- and (28). Arithmetic experimentation with material parameters showed that from the four roots in (29) only one provides an admissible solution. The stricter admissibility constraints, in this case, are the driving force to be positive, i.e, $f \geq 0$, and the sonic wave retains the material in the rarefied phase, i.e., $\gamma^+ \geq -\gamma_m$, for varying impactor velocity V and phase boundary velocity $\dot{s}$. This root is used later to make a map of all possible solutions. The stress profile with the jumps in the bar for two different instants for an impactor velocity $V_0 = 35$ m/s and a phase transition front velocity $\dot{s} = 45$ m/s is plotted in Fig. 6b.

5.1.4. Overdriven phase transition front

The last possibility is to have only one phase transition front propagating with supersonic speed ($\dot{s} \geq c_0$, the phase transition front is said to be overdriven), as seen in Fig. 4d. Two distinct regions exist in the continuum in this case. The first region is traversed by the supersonic phase transition wave ($0 < x < \dot{s}t$), and it lies in the densified phase under strain γ^- and moving with velocity V. The second region is the unperturbed material. This mode of deformation appears for strong impacts and it is analogous with the so-called "Shock mode" for foams in Zheng et al. (2012) or "Dynamic Mode" for two-dimensional honeycombs in Zheng et al. (2005) or the shock formation study in Gaitanaros and Kyriakides (2015). In mathematical form:

$$\gamma(x,t) = \begin{cases} \gamma^- & \text{for} \quad 0 < x < \dot{s}t \\ 0 & \text{for} \quad x > \dot{s}t \end{cases}, v(x,t) = \begin{cases} V & \text{for} \quad 0 < x < \dot{s}t \\ 0 & \text{for} \quad x > \dot{s}t \end{cases} \tag{30}$$

The unknowns in (30) are γ^- and $\dot{s}$ with the impactor velocity V being the parameter of the problem. Unlike the case with the sonic wave followed by the phase transition front, in the overdriven case the phase transition velocity $\dot{s}$ is calculated from the initial boundary value problem, and the solution is uniquely determined for a given impactor velocity V. Utilizing the kinematic and momentum jump conditions in (7) and (8), respectively, γ^- and $\dot{s}$ are found. Beginning with the jump condition in (7), $\dot{s}$ is:

$$[\![v]\!] = -\dot{s}[\![\gamma]\!] \Rightarrow \dot{s} = -\frac{V}{\gamma^-}, \tag{31}$$

and replacing (31) in (8), the stress behind the overdriven shock front is:

$$[\![\sigma]\!] = -\rho\dot{s}[\![v]\!] \Rightarrow \sigma^- = \rho\frac{V^2}{\gamma^-}. \tag{32}$$

The quadratic dependence of the stress on the impactor velocity V behind the shock front is verified also experimentally (Tan et al., 2005b; Li et al., 2007; Barnes et al., 2014; Petel et al., 2014; Gaitanaros and Kyriakides, 2015). Simplifying and rearranging terms in (32) leads to the following quartic equation for γ^-:

$$B(\gamma^-)^4 + (3B - \rho V^2)(\gamma^-)^3 + 3(B - \rho V^2)(\gamma^-)^2 + (A - 3\rho V^2)\gamma^- - \rho V^2 = 0. \tag{33}$$

There are potentially four roots for γ^-, out of which only one is admissible. The stricter constraint for admissibility, in this case, is the driving force to be positive. The stress profile with the jump in the bar for two different instants for an impactor velocity $V_0 = 55$ m/s ($\simeq c_0$) is plotted in Fig. 6c.

5.1.5. The totality of solutions for the compressive impact

As seen above, for the sonic wave followed by a transition front case, the solution is parametric in the impactor velocity V and the phase transition front velocity $\dot{s}$. In contrast, the pure shock wave in the rarefied phase and the overdriven case are parametric only in the impactor velocity V. The shock wave propagation case in the pre-strained densified phase is parametric in the impactor velocity V and the initial strain γ_i, but from Fig. 5 one notices that the dependence is trivial, i.e. there is always an admissible solution with the positive driving force for all values of V and $\gamma_i \leq -\gamma_M$. Hence, this case is not discussed further here. Keeping these points in mind, a map in the V–$\dot{s}$ plane is made to show the different admissible solutions that exist, i.e., the totality of solutions. This map serves the same purpose as, for example, a pressure-temperature phase transition diagram for water, in which for a given set of pressure and temperature, the reader is informed about the state of water, e.g. if it is in the solid phase, a liquid-vapor mixture, etc. The totality of solutions for Materials 1, 2, and 3 in Table 1 are presented in Fig. 7. Figs. 7a and b present the same qualitative behavior. The following observations can be made:

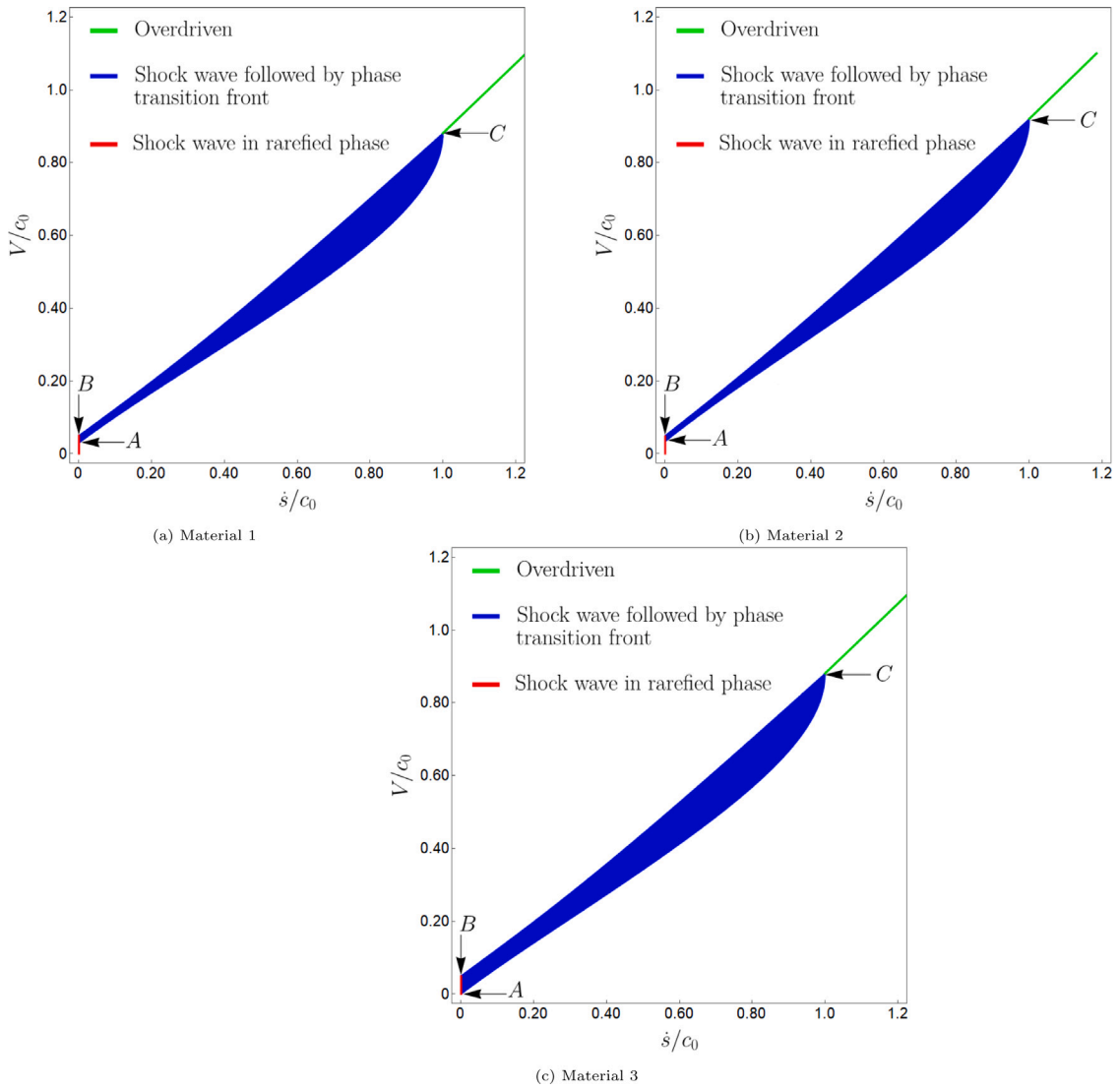

Fig. 7. Totality of solutions for the impact problem for (a) Material 1, and (b) Material 2 in Table 1.

1. There is a range of impactor velocities V up to point A, where only the sonic wave solution exists.
2. For impactor velocities V after point A until point B ($V = c_0\gamma_m$) a sonic wave followed by a phase transition solution can also exist in addition to the single sonic wave solution. This non-uniqueness can be remedied by having a *nucleation criterion* that sets a condition for the emergence of a phase transition front. If the nucleation criterion is satisfied then the solution with the shock wave followed by the phase transition front is chosen. The non-uniqueness arising due to the speed $\dot{s}$ being a parameter can be remedied by prescribing a *kinetic law* law that picks only one value of $\dot{s}$. The reader is referred to the Appendix for a specific example with numerical values.
3. Impactor velocities from point B to point C result only in the sonic wave followed by a phase transition solution. The non-uniqueness arising due to the speed $\dot{s}$ being a parameter can be remedied by prescribing a kinetic law that picks only one value of $\dot{s}$.
4. For impactor velocities higher than point C, the overdriven case is only possible, i.e., the supersonic phase transition. The solution is a uniquely defined function of the impactor velocity, and it appears to be linear, which is also observed in experiments (Barnes et al., 2014) and finite element simulations (Gaitanaros and Kyriakides, 2015). Note that the overdriven solution (green line) can be expanded into the subsonic domain of phase transition velocities $\dot{s}$. However, by definition, the overdriven case implies $\dot{s} \geq c_0$. In fact, this would correspond to the sonic wave plus phase transition front solution with $\gamma^+ = 0$ or $v^+ = 0$. The x–t plane in this case of Fig. 4c degenerates to Fig. 4d.

Fig. 7c, which depicts the totality of solutions for Material 3, has all the features above, but two solutions are possible at point A. This is understood by noticing that $U(-\gamma_M) < U(0) = 0$, which makes the phase transition favorable to happen directly without the need of higher impactor velocities. The non-uniqueness arising due to this can be remedied by having a nucleation criterion.

5.2. Decompressive impact

Now, attention is focused on the case of a decompressive impact where the impactor velocity is V to the left, like in Fig. 1b. The material exists under an initial strain γ_i and stress σ_i. This initial boundary value problem admits potentially six different solutions. Knowing that no more than two discontinuities can exist in the medium (Abeyaratne and Knowles, 2006), the six cases considered for the decompression problem are:

1. A sonic wave propagates in the pre-strained rarefied phase ($\gamma_i \geq -\gamma_m$), with the x–t plane as shown in Fig. 8a.

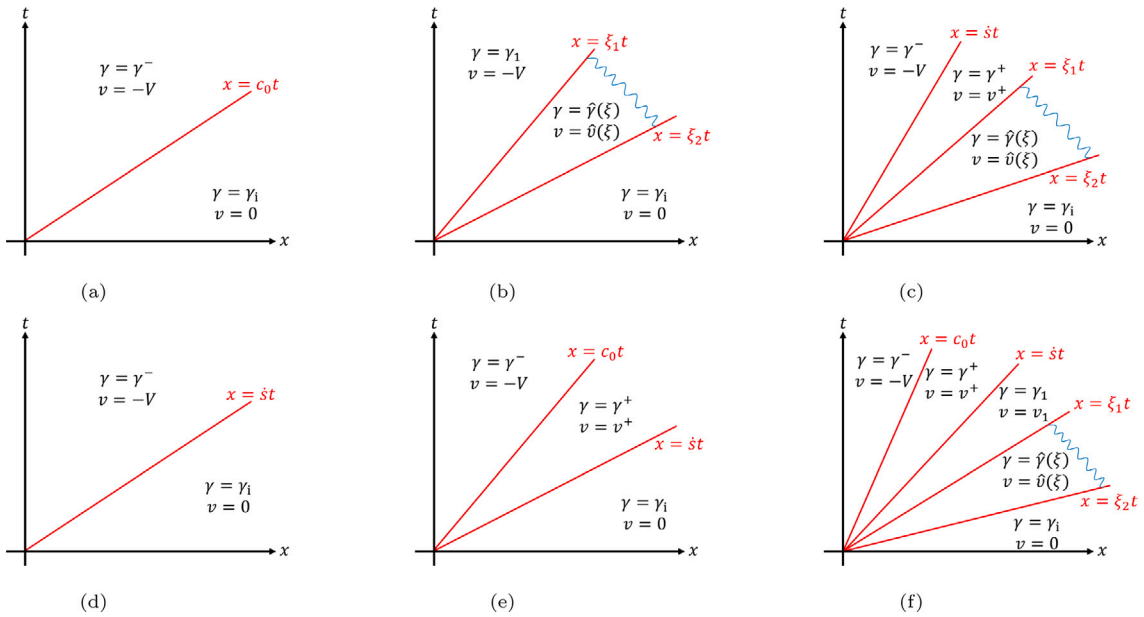

Fig. 8. The possible solutions of the decompressive impact problem for an initial strain γ_i: (a) A sonic wave propagating in the pre-strained rarefied phase, (b) a rarefaction wave (fan) propagating in the densified phase, (c) a fan followed by a phase transition front, (d) a single phase transition front, (e) a phase transition front followed by a sonic wave in the rarefied phase, and (d) a fan followed by a phase transition front followed by a sonic wave in the rarefied phase.

The remaining 5 cases are the more interesting ones and correspond to $\gamma_i \leq -\gamma_M$.

2. A rarefaction wave, also called fan, which is a discontinuity-free solution with the x–t plane as shown in Fig. 8b.
3. A rarefaction wave (fan) followed by a phase transition front transforming material from the densified to the rarefied phase with the x–t plane as shown in Fig. 8c.
4. A single phase transition front transforming material from the densified to the rarefied phase with the x–t plane as shown in Fig. 8d. It will be shown that this case can be considered as a special case of the fan followed by the phase transition front.
5. A phase transition front followed by a sonic wave with the x–t plane as shown in Fig. 8e. In this case, although admissible solutions are generated in the compression problem, it does not provide admissible solutions in the decompression case.
6. A rarefaction wave followed by a phase transition front followed by a sonic wave in the rarefied phase with the x–t plane as shown in Fig. 8f. This case is not solvable.

5.2.1. Sonic wave in the pre-strained rarefied phase

The sonic wave solution in a linear elastic medium, as outlined in Section 5.1.1, is applicable for decompressive impacts and $\gamma_i \geq -\gamma_m$, resulting in the following strain and particle velocity fields:

$$\gamma(x,t) = \begin{cases} \gamma_i + V/c_0 & \text{for } 0 < x < c_0 t \\ 0 & \text{for } x > c_0 t \end{cases}, v(x,t) = \begin{cases} -V & \text{for } 0 < x < c_0 t \\ 0 & \text{for } x > c_0 t \end{cases}. \tag{34}$$

This solution is dissipation free, and the only constraint on its applicability is the extent to which the linear behavior is legitimate for tensile strains. This case is not further discussed in this work because the focus here is on compression and decompression, not the tensile response.

5.2.2. Rarefaction wave (fan)

The material exists in the densified phase under strain γ_i and the decompressive impact causes the material to stretch. The slope of the characteristic lines of the wave equation in (5) in the x–t plane, calculated by $\sqrt{\sigma'(\gamma)/\rho}$, decreases during decompression. It is evident from the constitutive Eq. (14)c and Fig. 3a that $\sigma'(\gamma_i) > \sigma'(\gamma)$ for $\gamma_i < \gamma \leq -\gamma_M$. Hence, the wave front corresponding to the initial strain γ_i travels the fastest in the material with velocity ξ_2, and the wave front corresponding to strain γ_1, which strain is found from the solution of the IBVP, travels the slowest with velocity ξ_1. Hence, the result is a discontinuity-free wave decompressing the material, called a rarefaction wave. In the x–t plane there are infinite characteristic lines between $x = \xi_1 t$ and $x = \xi_2 t$ opening like a "fan", and that is why the solution is also called the "fan" solution. In the case where the stress–strain curve $\sigma(\gamma)$ was such that $\sigma'(\gamma_i) < \sigma'(\gamma)$ for $\gamma_i < \gamma \leq -\gamma_M$, then the back of the wave travels the fastest, meets with the front of the wave and generates a shock. Based on this explanation, Fig. 9 illustrates abstractly and more generally when a rarefaction wave (fan) or a shock wave can be created. Whether a rarefaction or a shock wave is generated, depends on the convexity of the stress–strain curve, and the direction it is traversed during a dynamic process.

As a continuous solution, the fan is a dissipation-free solution to the problem. Fan solutions of this type are discussed in (Knowles, 2002, 2003). In mathematical form:

$$\gamma(x,t) = \begin{cases} \gamma_1 & \text{for} \quad 0 \leq x \leq \xi_1 t \\ \hat{\gamma}(\xi) & \text{for} \quad \xi_1 t \leq x \leq \xi_2 t \\ \gamma_i & \text{for} \quad x \geq \xi_2 t \end{cases}, v(x,t) = \begin{cases} -V & \text{for} \quad 0 \leq x \leq \xi_1 t \\ \hat{v}(\xi) & \text{for} \quad \xi_1 t \leq x \leq \xi_2 t \\ 0 & \text{for} \quad x \geq \xi_2 t \end{cases} \tag{35}$$

Solution (35) is continuous, meaning that $\hat{\gamma}(\xi_1) = \gamma_1$ and $\hat{\gamma}(\xi_2) = \gamma_i$. Similarly, $\hat{v}(\xi_1) = -V$ and $\hat{v}(\xi_2) = 0$. The unknowns in (35) are the functions $\hat{v}(\xi)$, or equivalently $v(\gamma)$, and $\hat{\gamma}(\xi)$, as well as the constant γ_1; ξ_1 and ξ_2 can be found by demanding continuity of the solution. The impactor velocity V and the initial strain γ_i are the parameters of the problem. Using (2) and the chain rule, the following ordinary differential equation for the particle velocity $\hat{v}(\xi)$ and strain $\hat{\gamma}(\xi)$ arise in the case of a fan:

$$\hat{v}'(\xi) = -\xi \hat{\gamma}'(\xi). \tag{36}$$

The sonic wave speed in the densified phase, unlike the rarefied phase, is a function of the strain and it is given as:

$$c(\gamma) = \sqrt{\frac{d\sigma/d\gamma}{\rho}} = \frac{\Omega}{(1+\gamma)^2}, \qquad \text{where } \Omega = \sqrt{\frac{-3(A-B)}{\rho}}. \tag{37}$$

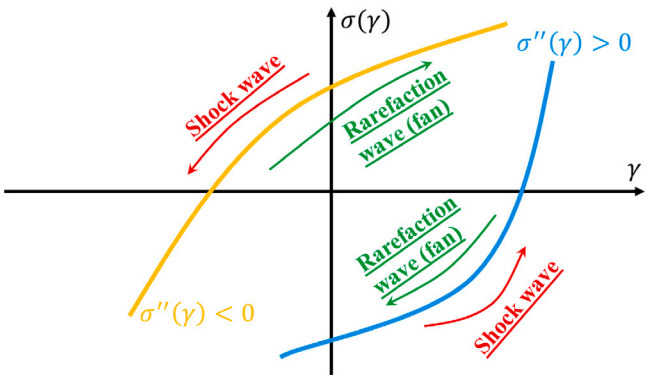

Fig. 9. Creation of rarefaction waves (fans) or shock waves depends on the convexity of the stress–strain curve and the direction it is traversed.

Applying the chain rule on the equation of motion (5), combining it with $c(\gamma)$ from (37) and using also (36), the following relation holds true for the fan:

$$c(\hat{\gamma}(\xi)) = \xi. \tag{38}$$

By requiring the solution to be continuous, ξ_1 and ξ_2 are calculated by (37) and (38):

$$\xi_1 = \frac{\Omega}{(1+\gamma_1)^2}, \tag{39}$$

$$\xi_2 = \frac{\Omega}{(1+\gamma_i)^2}. \tag{40}$$

Integrating (36), requiring that $\hat{v}(\xi_2) = 0$ and changing the integration variable $\xi \to \hat{\gamma}(\xi)$ while utilizing (38), the particle velocity is:

$$v(\gamma) = \left(\frac{1}{1+\gamma} - \frac{1}{1+\gamma_i}\right)\Omega. \tag{41}$$

Setting in (41)$\gamma = \gamma_1$ and from continuity $v(\gamma_1) = -V$, the resulting strain after the fan is:

$$\gamma_1 = -\frac{V(1+\gamma_i)+\gamma_i\Omega}{V(1+\gamma_i)-\Omega}. \tag{42}$$

From (37) and (38), $\hat{\gamma}(\xi)$ is derived:

$$\hat{\gamma}(\xi) = \pm\sqrt{\frac{\Omega}{\xi}} - 1, \tag{43}$$

where out of the two solutions, the one with the negative sign is rejected because it would result in $\gamma < -1$ and violate (3). The maximum impactor (decompression) velocity with which the continuum can be pulled and result in a fan solution is obtained by demanding:

$$\gamma_1(V) \le -\gamma_M \quad \Leftrightarrow \quad V \le \frac{\gamma_i + \gamma_M}{(1+\gamma_i)(\gamma_M - 1)}\Omega. \tag{44}$$

So, the maximum velocity with which the continuum can be pulled so that a fan solution is applicable depends on the initial strain of the material γ_i and tends to infinity as the material gets infinitely compacted. The region of admissible solutions for the fan case for Materials 1, 2 and 3 are presented in Fig. 10. Their qualitative characteristics are the same and only the hyperbola on the right-hand side of (44) changes.

5.2.3. What are the characteristics of discontinuities in the decompressive impact?

The rarefaction wave is a continuous solution, so no driving force or discontinuity velocity is involved in its solution. But, before the discontinuous solutions are presented, the discussion is diverted to the discussion of the qualitative characteristics the discontinuities should possess in the decompression problem. The geometric interpretation of the driving force and discontinuity velocity, as shown in Fig. 2, is employed to offer some understanding.

Fig. 11 presents the four cases which prohibit a discontinuity to exist in the decompressive impact problem. Fig. 11a presents the case where the discontinuity velocity is supersonic ($\dot{s} > c_0$). Although the driving force can be potentially positive ($A_2 - A_1 > 0$), the chord connecting the stresses and strains before and after the discontinuity does not intersect the rarefied linear phase, or intersects the linear phase at infinity, meaning that $\gamma^- \to +\infty$, hence it is rejected. It is also possible that for intense compaction, i.e., values of γ^+ near -1, the chord actually might intersect the linear phase for finite values of γ^-, but in that case, $A_2 = 0$, and the driving force is negative prohibiting the solution as seen in Fig. 11b. Consequently, in the decompressive impact problem, no discontinuity can propagate supersonically, i.e., $\dot{s} > c_0$, which is a very strong restriction. This is a byproduct of the linearity in the tensile region; if the linear behavior at small tensile strains is followed by a non-linear strain-stiffening behavior, then the two curves might intersect at a finite value of γ^-, and supersonic discontinuities can propagate in decompressive impact.

It is useful, at this point, to introduce the strain at which the projection of the linear phase intersects the densified phase curve which is denoted as γ^*. If the discontinuity propagates with exactly the sonic velocity $\dot{s} = c_0$, then for $\gamma^+ \neq \gamma^*$ the chord is parallel to the linear phase, and again $\gamma^- \to +\infty$ provides an inadmissible solution. For the special case of $\gamma^+ = \gamma^*$, a finite value of γ^- is attained, but as seen from Fig. 11c the driving force is negative ($f = -A_1 < 0$), and the solution is prohibited again. Again a non-linear tensile behavior can make this case admissible.

The case where the discontinuity propagates subsonically ($\dot{s} < c_0$) is investigated last. Fig. 11d presents the subsonic case where $\gamma^+ < \gamma^*$. In this case not only the chord does not intersect the rarefied case ($\gamma^- \to +\infty$), but it is also obvious from Fig. 11d that the driving force is negative. A non-linear tensile behavior cannot remedy this case. From the brief discussion of the geometrical interpretation of the solutions, it is found that the only possible scenario for a discontinuity to exist in the decompressive impact is if: (1) it propagates subsonically ($\dot{s} < c_0$), and (2) $\gamma^+ > \gamma^*$.

5.2.4. Rarefaction wave (fan) followed by phase transition

The phase transition front trails the end of the fan, which moves with velocity ξ_1, so the restriction $\dot{s} \le \xi_1$ arises. The continuum is composed of four different regions: (1) a rarefied material moving with velocity V to the left and being transversed by the fan and the phase transition front ($0 \le x < \dot{s}t$), (2) a densified region at strain γ^+ transversed only by the fan ($\dot{s}t < x \le \xi_1 t$), (3) the region included in the rarefaction wave where strains and particle velocities change continuously ($\xi_1 t \le x \le \xi_2 t$), and the pre-strained material ahead of the fan ($x \ge \xi_2 t$). In mathematical form:

$$\gamma(x,t) = \begin{cases} \gamma^- & \text{for} \quad 0 \le x < \dot{s}t \\ \gamma^+ & \text{for} \quad \dot{s}t < x \le \xi_1 t \\ \hat{\gamma}(\xi) & \text{for} \quad \xi_1 t \le x \le \xi_2 t \\ \gamma_i & \text{for} \quad x \ge \xi_2 t \end{cases}, v(x,t) = \begin{cases} -V & \text{for} \quad 0 \le x < \dot{s}t \\ v^+ & \text{for} \quad \dot{s}t < x \le \xi_1 t \\ \hat{v}(\xi) & \text{for} \quad \xi_1 t \le x \le \xi_2 t \\ 0 & \text{for} \quad x \ge \xi_2 t \end{cases} \tag{45}$$

The unknowns in (45) are γ^-, γ^+, and the functions $\hat{\gamma}(\xi)$ and $\hat{v}(\xi)$, or equivalently $v(\gamma)$. ξ_1, ξ_2, and v^+ are calculated by the continuity of the fan solution. The initial strain γ_i, impactor velocity V and the transition front velocity $\dot{s}$ are the parameters of the solution. The structure of the solution for the fan $x \ge \xi_1 t$ is the same as the one in Section 5.2.2:

$$v(\gamma) = \left(\frac{1}{1+\gamma} - \frac{1}{1+\gamma_i}\right)\Omega, \tag{46}$$

$$\gamma^+ = \frac{-(1+\gamma_i)v^+ + \gamma_i\Omega}{(1+\gamma_i)v^+ + \Omega}, \tag{47}$$

$$\hat{\gamma}(\xi) = \sqrt{\frac{\Omega}{\xi}} - 1, \tag{48}$$

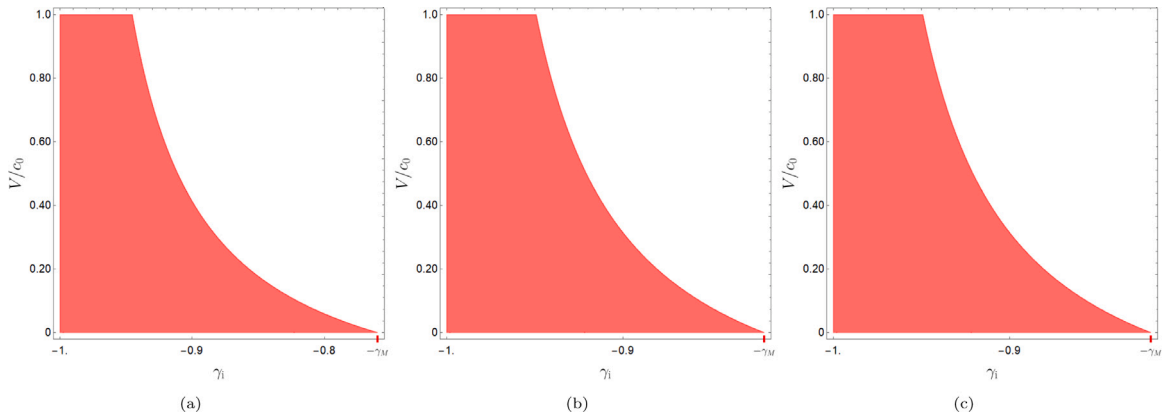

Fig. 10. Fan solution for the decompression impact problem for (a) Material 1, (b) Material 2, and (c) Material 3 in Table 1.

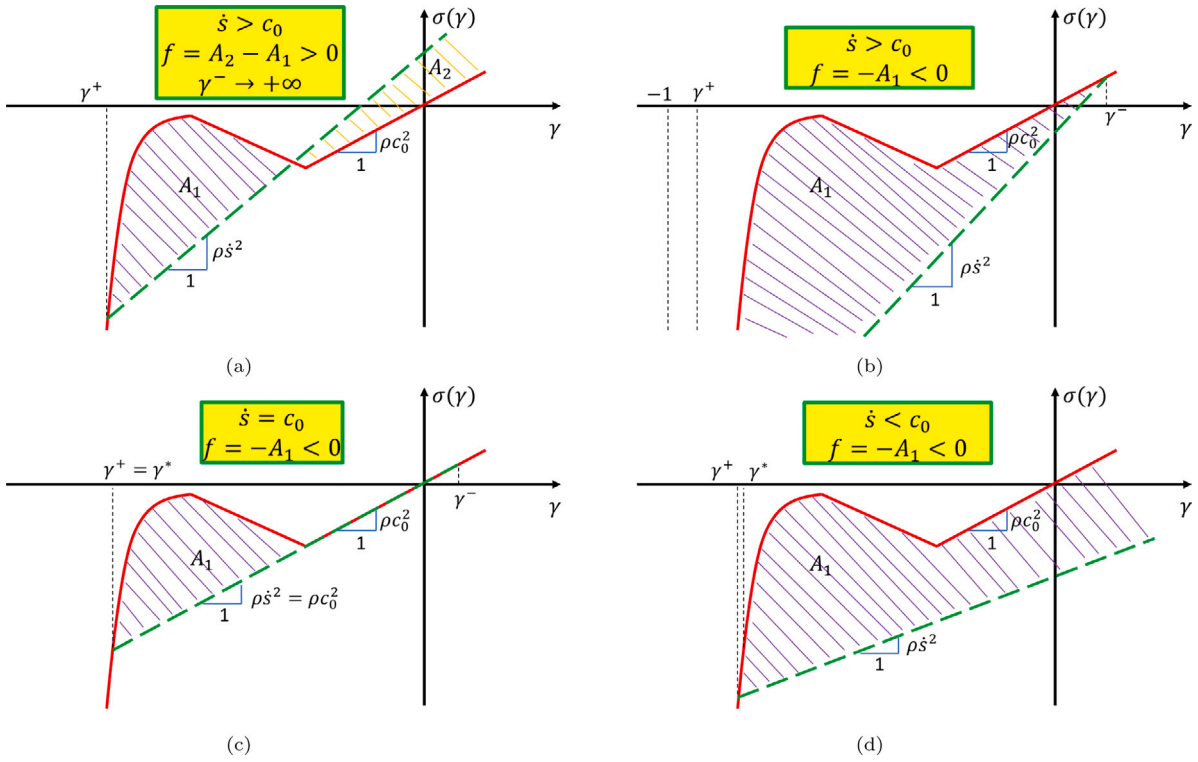

Fig. 11. The four *a priori* inadmissible cases for a discontinuity in the decompression problem.

$$\xi_1 = \frac{\Omega}{(\gamma^+ + 1)^2}, \tag{49}$$

$$\xi_2 = \frac{\Omega}{(\gamma_i + 1)^2}. \tag{50}$$

For the phase transition discontinuity the velocity jump condition (7) is used first and solved for γ^-:

$$[\![v]\!] = -\dot{s}[\![\gamma]\!] \Rightarrow \gamma^- = \frac{V + v^+ + \dot{s}\gamma^+}{s} \tag{51}$$

Then, the stress jump condition in (8) is:

$$[\![\sigma]\!] = -\rho\dot{s}[\![v]\!] \Rightarrow \frac{A - B}{(1+\gamma^+)^3} + B - E\gamma^- = -\rho\dot{s}(v^+ + V), \tag{52}$$

and replacing γ^- from (51), a quartic polynomial for γ^+ is solved. Out of the four roots, only one provides admissible solutions with the driving force positive and $\gamma^+ \leq -\gamma_M$ being the strictest constraints. Figs. 12a and b show the V–γ_i plane for the fan followed by a phase transition problem in decompression for Material 1 and 2, respectively. The solution is parametric in V, γ_i, and $\dot{s}$, i.e., it is a three-dimensional region in the V–γ_i–$\dot{s}$ space. The (blue) region in Figs. 12a and b is merely the projection of the three-dimensional region on the V–γ_i plane with $\dot{s}$ increasing as shown by the yellow arrow. In Figs. 12c and d, the solution is plotted together with the pure fan case. It is obvious that these two solutions are enough to guarantee that there is always an admissible solution to the decompression problem for a material pre-strained with a strain of γ_i and decompressed at a velocity V. Note that an admissible solution can exist even for $V = 0$. The pure fan solution for $V = 0$ is trivial; the fan followed by phase transition front solution can be eliminated for $V = 0$ by invoking a nucleation criterion.

5.2.5. *Single phase transition front*

Another solution is to have only one phase transition front from the densified to rarefied phase, as seen in Fig. 8d. Two distinct regions exist in the continuum in this case. The first region is traversed by the phase transition wave ($0 < x < \dot{s}t$), and it lies in the rarefied phase under strain γ^- and moving with velocity $-V$. The second region is

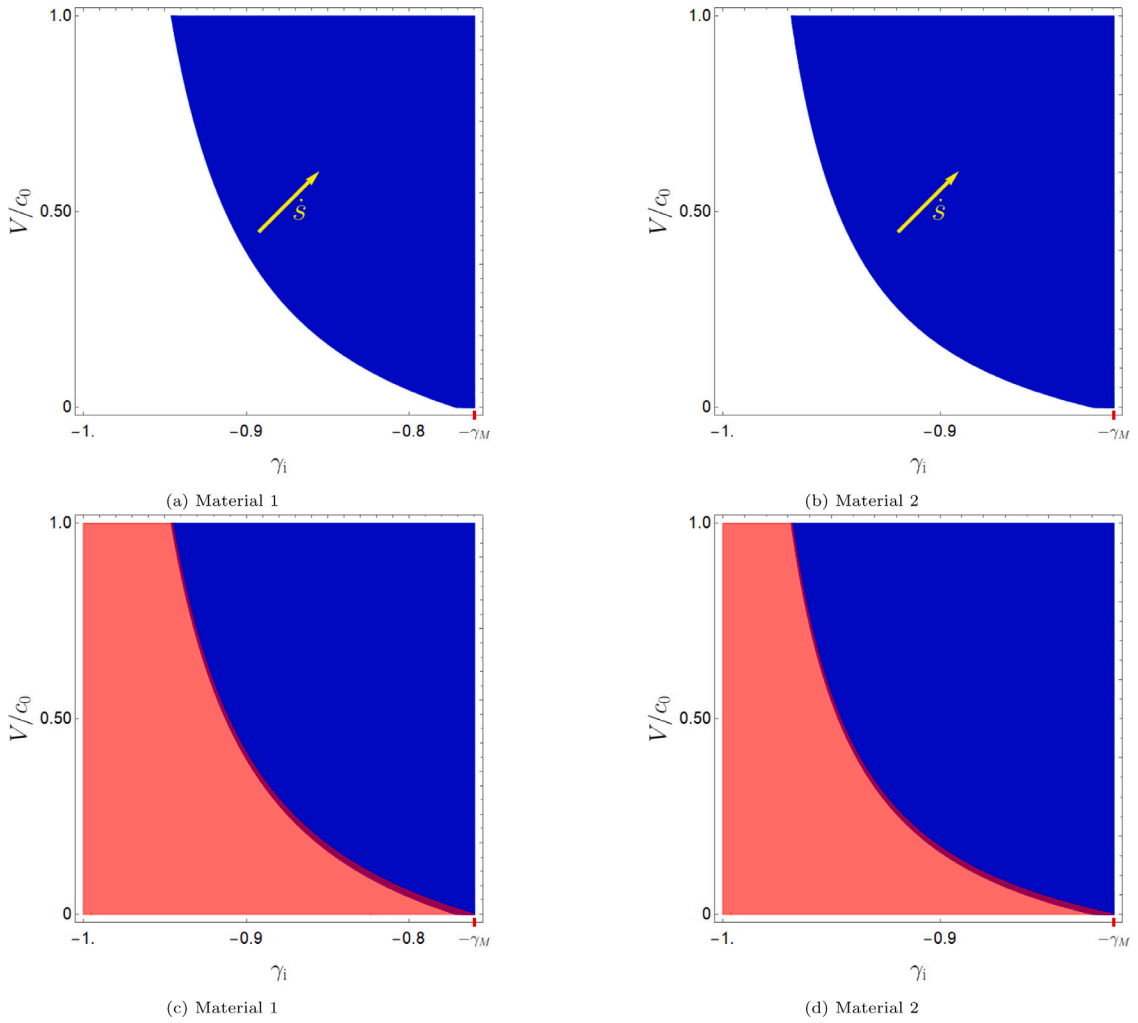

Fig. 12. Projection of the fan followed by a phase transition front solution for the decompression impact problem for (a) Material 1, and (b) Material 2 in Table 1. The solution (blue) is plotted together with the pure fan case (red) for (c) Material 1, and (d) Material 2.

the originally strained material in the densified phase under the initial strain γ_i and stress $\sigma_i = \sigma(\gamma_i)$. In mathematical form:

$$\gamma(x,t) = \begin{cases} \gamma^- & \text{for} \quad 0 < x < \dot{s}t \\ \gamma_i & \text{for} \quad x > \dot{s}t \end{cases}, v(x,t) = \begin{cases} -V & \text{for} \quad 0 < x < \dot{s}t \\ 0 & \text{for} \quad x > \dot{s}t \end{cases} \tag{53}$$

The unknowns in (53) are γ^- and $\dot{s}$, while the impactor velocity V and the initial strain are free parameters. Utilizing the velocity and stress jump conditions in (7) and (8), respectively, γ^- and $\dot{s}$ are found. Starting with the jump condition in (7), $\dot{s}$ is calculated:

$$[\![v]\!] = -\dot{s}[\![\gamma]\!] \Rightarrow \dot{s} = -\frac{V}{\gamma_i - \gamma^-}. \tag{54}$$

Replacing (54) in (8), simplifying, and rearranging terms leads to the following quadratic equation which provides two roots for γ^-:

$$E\gamma^{-2} - (\sigma_i + E\gamma_i)\gamma^- + \sigma_i\gamma_i - \rho V^2 = 0, \tag{55}$$

and the roots are:

$$\gamma^- = \frac{E\gamma_i + \sigma_i \pm \sqrt{(E\gamma_i - \sigma_i)^2 + 4E\rho V^2}}{2E}. \tag{56}$$

The solution corresponding to the minus root results in strains $\gamma^- \leq \gamma_i$, which is unrealistic, and hence disqualifies as a solution to the problem. Hence, the solution for γ^- for the single transition front case in the decompression problem is:

$$\gamma^- = \frac{E\gamma_i + \sigma_i + \sqrt{(E\gamma_i - \sigma_i)^2 + 4E\rho V^2}}{2E}. \tag{57}$$

Figs. 13a and b depict the admissible solutions for the single transition front case plotted together with the fan followed by the phase transition solution for Materials 1 and 2, respectively. On the V–γ_i plane, the latter is entirely encompassed by the former. Moreover, Figs. 13c and d present the solutions on the corresponding V–$\dot{s}$ planes for specific values of γ_i. Again, one can notice that the solution of the single phase transition front exists within the domain of the fan followed by the phase transition solution. Observation of the x–t planes in Fig. 8c and d makes clear that the single phase transition front x–t plane in Fig. 8d is a degenerated version of the x–t plane in Fig. 8c provided that $v^+ = 0$ or $\gamma^+ = \gamma_i$ or $\xi_1 = \xi_2$. Indeed, in the set of Eqs. (46)–(50), replacing one of the three conditions, the other two are automatically satisfied and the single phase transition solution is retrieved. Consequently, unlike the compression case, in decompressive impact, a single phase transition front solution does not add new solutions to the problem, and hence it will not be discussed further.

The remaining two candidate solutions to the problem fail to provide any admissible solution at all. The first one is the phase transition front followed by a sonic wave in the rarefied phase, and the second one is the fan followed by a phase transition front followed by a sonic wave in the rarefied phase. Each of them is discussed separately below and an explanation for why they are not admissible is provided.

5.2.6. *Phase transition front followed by a sonic wave in the rarefied phase*

Consider a propagating phase transition front from the densified to the rarefied phase followed by a sonic wave both sides of which are

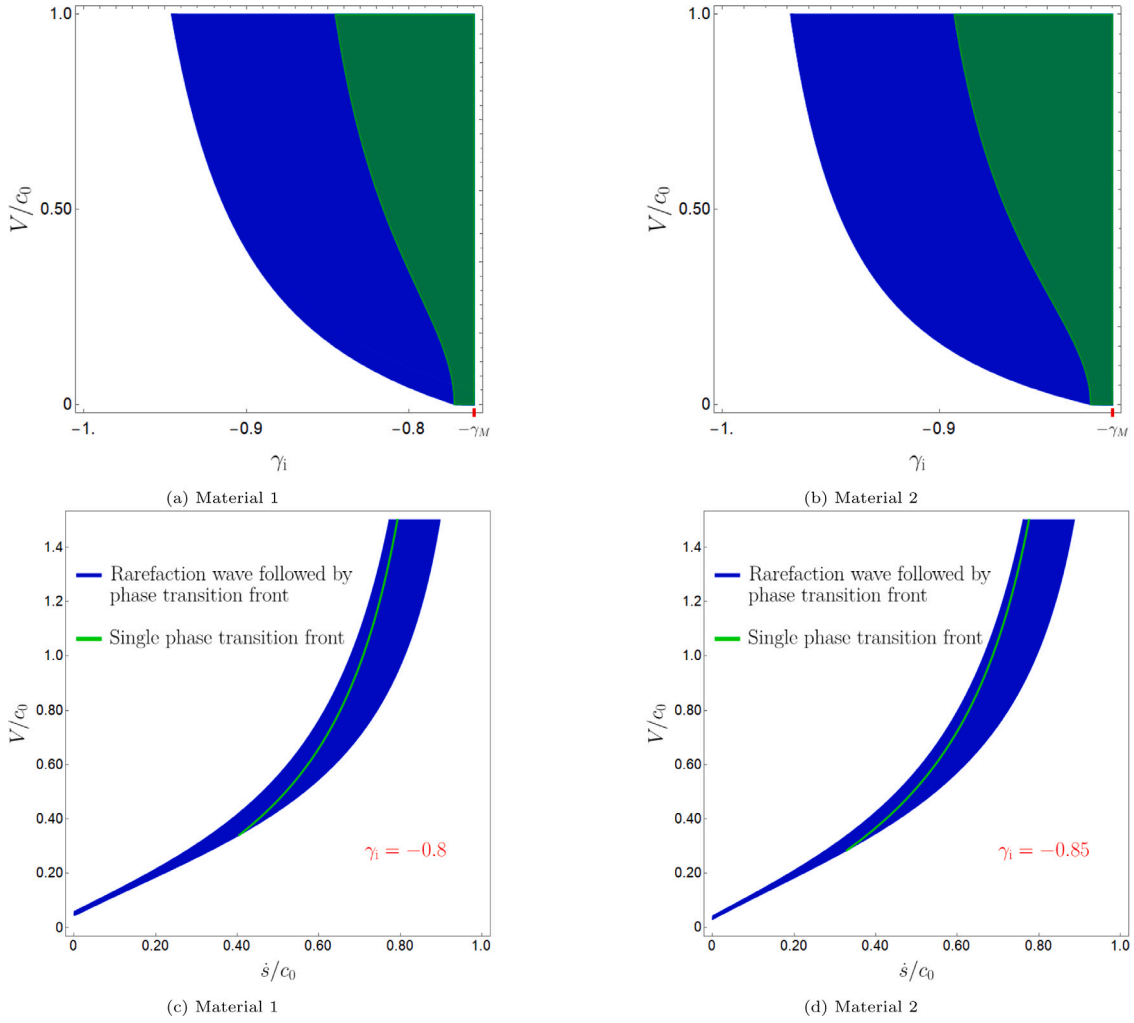

Fig. 13. Admissible solutions for the single phase transition front plotted together with the fan followed by the phase transition solution for (a) Material 1, and (b) Material 2 on the V–γ_i plane. (c) and (d) the corresponding solutions on V–$\dot{s}$ plane for specific values of γ_i.

in the rarefied phase, as seen in Fig. 8e. The phase transition front propagates with a supersonic velocity, i.e. $\dot{s} \geq c_0$. As discussed in Section 5.2.3 the supersonic (or even sonic) discontinuity propagation is not admissible in the decompressive impact. Nevertheless, the analysis for the supersonic phase transition front followed by a sonic wave is presented, because if the linear rarefied phase is changed to a nonlinear behavior, this case will generate permissible solutions. In that scenario, the phase transition front will be followed by a shock, and not a sonic, wave.

In the continuum, for the phase transition front followed by a sonic wave case, three distinct regions are observed at any moment. The first region is already transversed by the shock wave and the phase transition front ($0 < x < c_0 t$), and lies in the rarefied phase. All the material points move with velocity V and the strain is γ^-. The second region is transversed only by the transition front ($c_0 t < x < \dot{s}t$) and it is in the rarefied phase. Lastly is the pre-strained material ($x > \dot{s}t$). In mathematical form:

$$\gamma(x,t) = \begin{cases} \gamma^- & \text{for} \quad 0 < x < c_0 t \\ \gamma^+ & \text{for} \quad c_0 t < x < \dot{s}t \\ \gamma_i & \text{for} \quad x > \dot{s}t \end{cases}, v(x,t) = \begin{cases} V & \text{for} \quad 0 < x < ct \\ v^+ & \text{for} \quad ct < x < \dot{s}t \\ 0 & \text{for} \quad x > \dot{s}t \end{cases} \tag{58}$$

The unknowns in (58) are γ^+, γ^-, v^+ and the impactor velocity V, the phase transition front speed $\dot{s}$, as well as, the initial strain γ_i are parameters of the problem. Employing the kinematic jump condition in (7) for the sonic wave discontinuity results in:

$$[\![v]\!] = -\dot{s}[\![\gamma]\!] \Rightarrow v^+ = -V + c_0(\gamma^- - \gamma^+). \tag{59}$$

For the phase transition discontinuity, utilizing the velocity jump condition in (7) and replacing v^+ from (59):

$$[\![v]\!] = -\dot{s}[\![\gamma]\!] \Rightarrow \gamma^- = \frac{V + s\gamma_i + \gamma^+(c_0 - \dot{s})}{c_0}. \tag{60}$$

Then, using the stress jump conditions in (8) for the phase transition discontinuity combined with (59) and (60):

$$[\![\sigma]\!] = -\rho\dot{s}[\![v]\!] \Rightarrow \gamma^+ = \frac{\sigma_i - \dot{s}^2\gamma_i\rho}{E - s^2\rho}. \tag{61}$$

5.2.7. *Fan followed by a phase transition front followed by a shock wave in the rarefied phase*

The last case considered is that of a fan followed by a phase transition front followed by a shock wave in the rarefied phase, as seen in Fig. 8e. This is the most complex of all cases. The same considerations for the admissibility of the solutions made in 5.2.3 regarding the supersonic propagation of discontinuities, apply here too because the supersonic phase transition front followed by the sonic wave is included

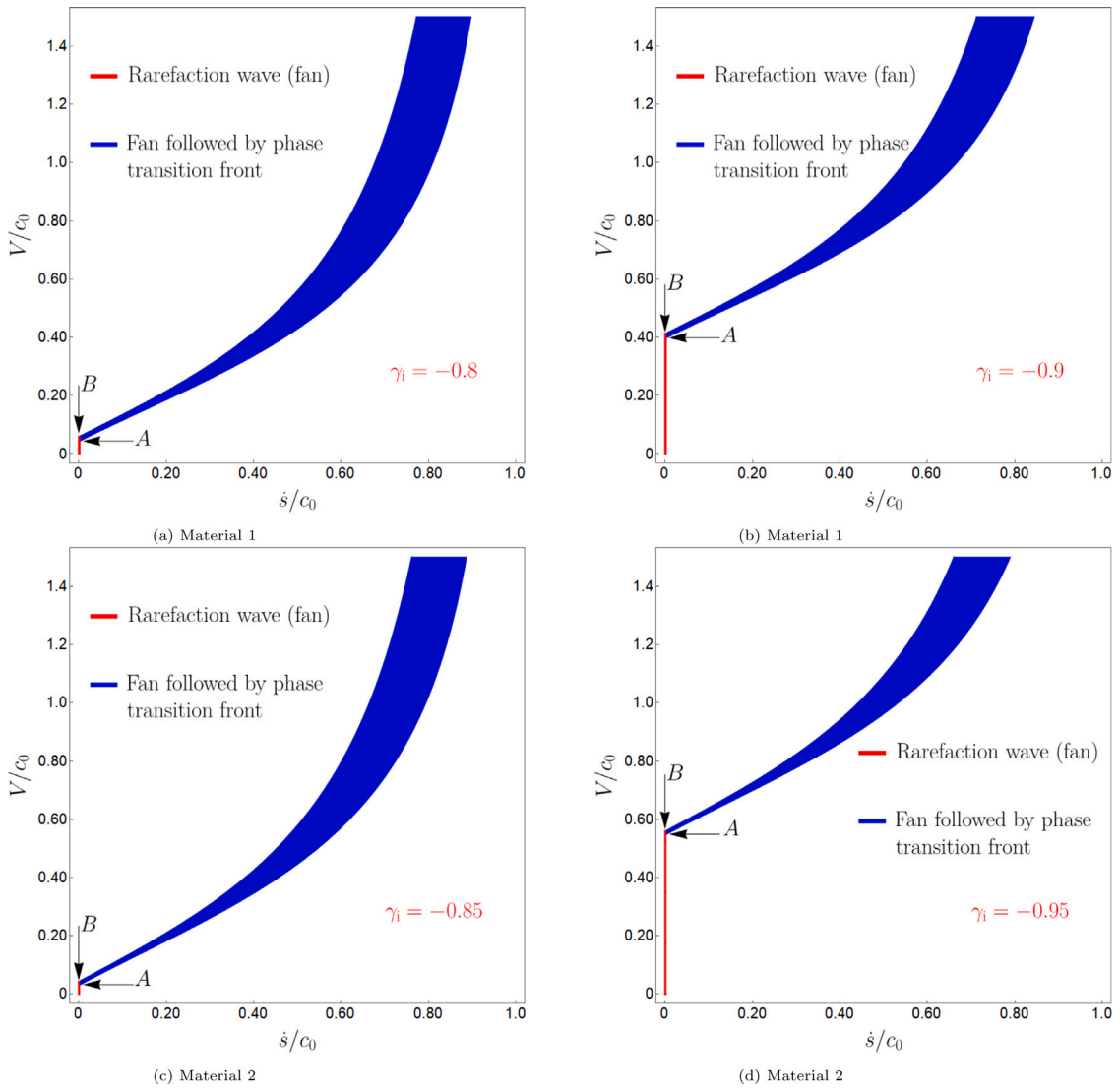

Fig. 14. Totality of solutions for Material 1 with initial strain (a) $\gamma_i = -0.8$, (b) $\gamma_i = -0.9$ and Material 2 with (c) $\gamma_i = -0.85$, (d) $\gamma_i = -0.95$.

in this case. In mathematical form:

$$\gamma(x,t) = \begin{cases} \gamma^- & \text{for} \quad 0 < x < c_0 t \\ \gamma^+ & \text{for} \quad c_0 t < x < \dot{s}t \\ \gamma_1 & \text{for} \quad \dot{s}t < x \le \xi_1 t \\ \hat{\gamma}(\xi) & \text{for} \quad \xi_1 t \le x \le \xi_2 t \\ \gamma_i & \text{for} \quad x \ge \xi_2 t \end{cases}, v(x,t) = \begin{cases} -V & \text{for} \quad 0 < x < c_0 t \\ v^+ & \text{for} \quad c_0 t < x < \dot{s}t \\ v_1 & \text{for} \quad \dot{s}t < x \le \xi_1 t \\ \hat{v}(\xi) & \text{for} \quad \xi_1 t \le x \le \xi_2 t \\ 0 & \text{for} \quad x \ge \xi_2 t \end{cases} \tag{62}$$

From the fan solution in Section 5.2.2, the strain $\hat{\gamma}(\xi)$ and velocity $v(\gamma)$ fields are known and can be used to calculate γ_1 and velocity v_1 after the fan as a function of ξ_1:

$$\gamma_1 = \sqrt{\frac{\Omega}{\xi_1}} - 1, \tag{63}$$

$$v_1 = \left(\frac{1}{1+\gamma_1} - \frac{1}{1+\gamma_i} \right) \Omega. \tag{64}$$

Therefore, the four unknowns are ξ_1, γ^-, γ^+, and v^+, while the impactor velocity V, the phase transition velocity $\dot{s}$ and the initial strain γ_i are parameters of the solution. The jump conditions in the phase transition give two equations. Another equation is obtained from the sonic wave jump condition. So, the system has three equations and four unknowns, hence it is undetermined. A limiting case is when the densified phase is not concave during compression, but linear or even convex. Then, the fan will turn into a discontinuity and it is proven that in any medium there are maximum two discontinuities that can exist at the same time (Abeyaratne and Knowles, 2006). Therefore, this class of solutions to the impact problem is ruled out.

5.2.8. *The totality of solutions for the decompressive impact*

Fig. 14 presents the totality of solutions for the decompressive impact. Out of the six possible solutions mentioned at the beginning of the discussion, eventually, only two qualify for plotting, the rest being disqualified for various reasons. If the material in the rarefied phase was not linear, but stain-stiffening at least one more solution (i.e., phase transition front followed by shock wave) could be possible.

From Figs. 14a and c, one notes that for initial strains γ_i closer to $-\gamma_M$ the fan solution is applicable for a small range of impactor velocities and the fan followed by the phase transition case appears early. This is because for smaller compressive strains the material is closer to the strain γ^* (projection of the rarefied stress–strain curve to the densified one), and phase transition is easier, see Section 5.2.3. In contrast, when the material is intensely compacted, Figs. 14b and d, it starts further from γ^*, the fan solution has a wider range of applicability, and the fan followed by the phase transition requires stronger (decompressive) impacts. Essentially, the fan assists the material to decompress to a favorable strain such that phase transition can take

place. In all cases though, there is a region of decompressive velocities between points A and B where both solutions are possible. Finally, one can notice the asymptotic behavior of the fan followed by the phase transition solution as $\dot{s} \to c_0$. As it was found from the geometrical interpretation of the problem in Section 5.2.3, no discontinuity, the phase transition in this case, can propagate supersonically, not even sonically, in the decompressive impact problem with linear rarefied phase. This strong restriction can be mitigated if the linear behavior is changed to a non-linear one.

6. Conclusions

Compressive and decompressive impact of porous meta-materials is investigated in this paper. The porous materials are assumed to have the ability to recover their initial configuration after cycles of (dynamic) loading/unloading. The materials are modeled using a continuum theory of phase transitions (Abeyaratne and Knowles, 2006) and the dynamical behavior is shown to involve propagating shocks, phase boundaries, and rarefaction waves (fans). Some of the solutions discussed are similar to those already described in the literature such as Zheng et al. (2012) and Gaitanaros and Kyriakides (2015), but others, such as the fan solutions, have not been described at length before. The compressive impact case is well-studied with an abundance of experimental data in the literature, while decompressive impact has received minimum theoretical and little experimental attention (to the best of the authors' knowledge). The analysis and results provided in this work can guide future theoretical and experimental efforts investigating the decompressive impact response of porous meta-materials. Maps have been constructed to show all possible, or totality of solutions to impact problems on these materials. These maps depict regions in which multiple solutions to the impact problem are possible. The non-uniqueness in the solutions can be remedied by adding a nucleation criterion and kinetic law for phase boundaries to the constitutive description. The kinetic relation is of the form $\dot{s} = \phi(f)$ and the nucleation criterion can be for example that f needs to be greater than a lower bound value for an interface to nucleate (Abeyaratne and Knowles, 2006; Knowles, 1999). This is left to future work. The analysis described here may be applicable to various types of porous materials, such as foams (Tan et al., 2005a), fiber networks (Picu and Ganghoffer, 2019), truss meta-structures (like Schaedler et al., 2011; Ozdemir et al., 2016), and a broader class of architectured materials (like Al-Ketan and Abu Al-Rub, 2019).

Declaration of competing interest

The authors declare no competing interest.

Data availability

No data was used for the research described in the article.

Acknowledgments

Research reported in this publication was supported through a seed grant from Penn's Materials Research Science and Engineering Center (MRSEC) DMR-1720530, USA.

Appendix. Retrieving unique solution from kinetic relation and nucleation criterion

In this Appendix, a kinetic relation and a nucleation criterion are used to alleviate the nonuniqueness of solutions in the case of a sonic wave followed by a phase transition front. The kinetic relation is of the form $\dot{s} = \phi(f)$. The nucleation criterion adopted is that in order for the densified phase to nucleate, the driving force must be higher than a critical value, called f_{n}. This is similar to saying that in order for the transition to happen an energy barrier must be surpassed first. The kinetic relation assumed here is just a linear function of the form $\dot{s} = \alpha(f - f_{\mathrm{n}})$. The kinetic relation and the nucleation criterion are shown in Fig. A.15a. The nucleation driving force is a material parameter and here for demonstration reasons, it is taken to be $f_{\mathrm{n}} = 30$ kPa. The proportionality constant α is the mobility of the phase boundary and it is varied in the results presented below. It has units of velocity over stress, i.e. [m/s/Pa]. Material 1 is used from Table 1.

Since the kinetic relation and the nucleation criterion specify uniquely a solution given an impactor velocity V, we will consider three different impactor velocity cases, as presented in Fig. A.15b, to demonstrate how to make use of them:

- $V = 1.8$ m/s *or* $V/c_0 = 0.032$. In this case, the driving force from the sonic wave followed by the phase transition front with $\dot{s} \to 0$ is less than f_{n}, so the densified phase cannot nucleate, and the sonic wave solution in (23) is admitted. This is an example of how the nucleation criterion remedies the non-uniqueness. A lower nucleation value of f_{n} could allow the nucleation of the densified phase.
- $V = 2.0$ m/s *or* $V/c_0 = 0.036$. In this case, the driving force from the sonic wave followed by the phase transition front with $\dot{s} \to 0$ is higher than f_{n}, so the densified phase nucleates at the left end of the bar, and the two-wave solution in (26) is admitted. In the next case, the methodology to alleviate the nonuniqueness with the kinetic relation is presented.

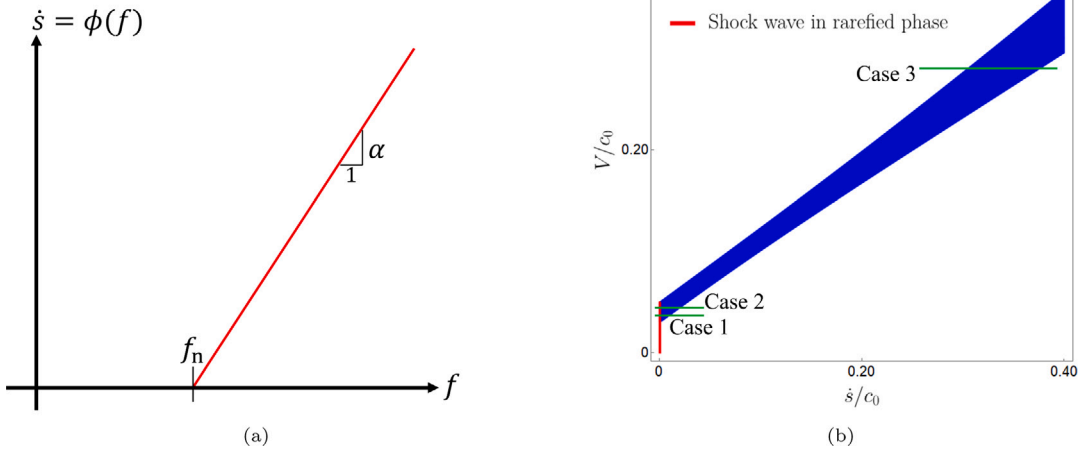

Fig. A.15. (a) Kinetic relation and nucleation criterion assumed in this work. (b) The three different impactor velocities cases considered.

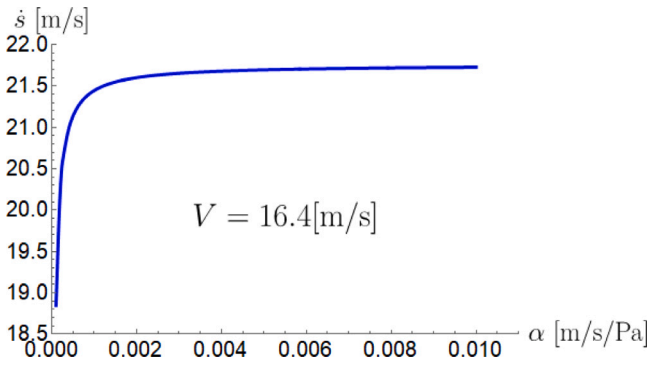

Fig. A.16. Parametric study of the influence of mobility on the phase transition velocity $\dot{s}$ for an impactor velocity of $V = 16.4$ m/s.

- $V = 16.4$ m/s *or* $V/c_0 = 0.3$. In this case, the driving force from the sonic wave followed by the phase transition front is higher than f_n, so the densified phase nucleates at the left end of the bar, and the two-wave solution in (26) is admitted. The unknowns in (26) are γ^+, γ^-, v^+, and $\dot{s}$ while the impactor velocity V is the only parameter of the problem. The available equations, as shown in Section 5.1.2, are:

$$[\![v]\!] = -\dot{s}[\![\gamma]\!] \Rightarrow v^+ = -c_0\gamma^+, \tag{A.1}$$

$$[\![v]\!] = -\dot{s}[\![\gamma]\!] \Rightarrow \gamma^+ = \frac{V + \dot{s}\gamma^-}{\dot{s} - c_0}, \tag{A.2}$$

$$c\rho\dot{s}(\gamma^-)^4 + \{B + \rho[3c\dot{s} + (c+\dot{s})V]\}(\gamma^-)^3 + 3\{B + \rho[\dot{s}V + c(V+\dot{s})]\}(\gamma^-)^2 + \{3B + \rho[c\dot{s} + 3V(c+\dot{s})]\}\gamma^- + (c+\dot{s})\rho V + A = 0, \tag{A.3}$$

$$\dot{s} = \alpha(f - f_n). \tag{A.4}$$

This is a system of four equations with four unknowns. Given an impactor velocity, the solution is uniquely defined. Fig. A.16 is a parametric study of the mobility to the discontinuity velocity $\dot{s}$ and the resulting strain in the densified phase. A two-order-of-magnitude variation is considered. Like the nucleation driving force f_n, mobility α is a material parameter.

References

Abeyaratne, R., Knowles, J.K., 1990. On the driving traction acting on a surface of strain discontinuity in a continuum. J. Mech. Phys. Solids 38 (3), 345–360.

Abeyaratne, R., Knowles, J.K., 2000. On a shock-induced martensitic phase transition. J. Appl. Phys. 87 (3), 1123–1134.

Abeyaratne, R., Knowles, J.K., 2006. Evolution of Phase Transitions: A Continuum Theory. Cambridge University Press.

Agrawal, V., Bhattacharya, K., 2014. Shock wave propagation through a model one dimensional heterogeneous medium. Int. J. Solids Struct. 51 (21), 3604–3618.

Agrawal, V., Bhattacharya, K., 2018. Impact induced depolarization of ferroelectric materials. J. Mech. Phys. Solids 115, 142–166.

Al-Ketan, O., Abu Al-Rub, R.K., 2019. Multifunctional mechanical metamaterials based on triply periodic minimal surface lattices. Adv. Eng. Mater. 21 (10), 1900524.

Babaee, S., Shahsavari, A.S., Wang, P., Picu, R.C., Bertoldi, K., 2015. Wave propagation in cross-linked random fiber networks. Appl. Phys. Lett. 107 (21), 211904.

Barnes, A., Ravi-Chandar, K., Kyriakides, S., Gaitanaros, S., 2014. Dynamic crushing of aluminum foams: Part I – experiments. Int. J. Solids Struct. 51 (9), 1631–1645.

Butt, H., Rajesekharan, R., Dai, Q., Sarfraz, S., Vasant Kumar, R., Amaratunga, G.A.J., Wilkinson, T.D., 2012. Cylindrical Fresnel lenses based on carbon nanotube forests. Appl. Phys. Lett. 101 (24), 243116.

Cao, A., Dickrell, P.L., Sawyer, W.G., Ghasemi-Nejhad, M.N., Ajayan, P.M., 2005. Super-compressible foamlike carbon nanotube films. Science 310 (5752), 1307–1310.

Coleman, J.N., Khan, U., Blau, W.J., Gun'ko, Y.K., 2006. Small but strong: A review of the mechanical properties of carbon nanotube–polymer composites. Carbon 44 (9), 1624–1652.

Dattelbaum, D.M., Ionita, A., Patterson, B.M., Branch, B.A., Kuettner, L., 2020. Shockwave dissipation by interface-dominated porous structures. AIP Adv. 10 (7), 075016.

Deshpande, V., Fleck, N., 2000. High strain rate compressive behaviour of aluminium alloy foams. Int. J. Impact Eng. 24 (3), 277–298.

Escobar, J., Clifton, R., 1993. On pressure-shear plate impact for studying the kinetics of stress-induced phase transformations. Mater. Sci. Eng. A 170 (1), 125–142.

Eshelby, J.D., 1951. The force on an elastic singularity. Philos. Trans. R. Soc. Lond. Ser. A 244 (877), 87–112.

Frenzel, T., Findeisen, C., Kadic, M., Gumbsch, P., Wegener, M., 2016. Tailored buckling microlattices as reusable light-weight shock absorbers. Adv. Mater. 28 (28), 5865–5870.

Gaitanaros, S., Kyriakides, S., 2014. Dynamic crushing of aluminum foams: Part II – analysis. Int. J. Solids Struct. 51 (9), 1646–1661.

Gaitanaros, S., Kyriakides, S., 2015. On the effect of relative density on the crushing and energy absorption of open-cell foams under impact. Int. J. Impact Eng. 82, 3–13, Metallic Foams under Dynamic Loading.

Garyfallogiannis, K., Ramanujam, R.K., Litvinov, R.I., Yu, T., Nagaswami, C., Bassani, J.L., Weisel, J.W., Purohit, P.K., Tutwiler, V., 2023. Fracture toughness of fibrin gels as a function of protein volume fraction: Mechanical origins. Acta Biomater.

Gibson, L.J., Ashby, M.F., 1997. Cellular Solids: Structure and Properties, second ed. In: Cambridge Solid State Science Series, Cambridge University Press.

Gurtin, M.E., Fried, E., Anand, L., 2010. The Mechanics and Thermodynamics of Continua. Cambridge University Press.

Hawreliak, J.A., Lind, J., Maddox, B., Barham, M., Messner, M., Barton, N., Jensen, B., Kumar, M., 2016. Dynamic behavior of engineered lattice materials. Sci. Rep. 6 (1), 28094.

Herrmann, W., 1969. Constitutive equation for the dynamic compaction of ductile porous materials. J. Appl. Phys. 40 (6), 2490–2499.

Hutchens, S.B., Needleman, A., Greer, J.R., 2012. A microstructurally motivated description of the deformation of vertically aligned carbon nanotube structures. Appl. Phys. Lett. 100 (12), 121910.

Jang, W.-Y., Kyriakides, S., 2009a. On the crushing of aluminum open-cell foams: Part I. Experiments. Int. J. Solids Struct. 46 (3), 617–634.

Jang, W.-Y., Kyriakides, S., 2009b. On the crushing of aluminum open-cell foams: Part II analysis. Int. J. Solids Struct. 46 (3), 635–650.

Jin, L., Khajehtourian, R., Mueller, J., Rafsanjani, A., Tournat, V., Bertoldi, K., Kochmann, D.M., 2020. Guided transition waves in multistable mechanical metamaterials. Proc. Natl. Acad. Sci. 117 (5), 2319–2325.

Kader, M., Islam, M., Hazell, P., Escobedo, J., Saadatfar, M., Brown, A., Appleby-Thomas, G., 2016. Modelling and characterization of cell collapse in aluminium foams during dynamic loading. Int. J. Impact Eng. 96, 78–88.

Khajehtourian, R., Kochmann, D.M., 2020. Phase transformations in substrate-free dissipative multistable metamaterials. Extreme Mech. Lett. 37, 100700.

Kim, O., Liang, X., Litvinov, R., Weisel, J., Alber, M., Purohit, P., 2015. Foam-like compression behavior of fibrin networks. Biomech. Model. Mechanobiol. 15.

Knowles, J., 1999. Stress-induced phase transitions in elastic solids. Comput. Mech. 22, 429–436.

Knowles, J.K., 2002. Impact-induced tensile waves in a rubberlike material. SIAM J. Appl. Math. 62, 1153–1175.

Knowles, J.K., 2003. Sudden tensile loading of a rubberlike bar. Mech. Res. Commun. 30 (6), 581–587.

Kuzumaki, T., Mitsuda, Y., 2006. Nanoscale mechanics of carbon nanotube evaluated by nanoprobe manipulation in transmission electron microscope. Japan. J. Appl. Phys. 45 (1R), 364.

Lakes, R., Rosakis, P., Ruina, A., 1993. Microbuckling instability in elastomeric cellular solids. J. Mater. Sci. 28 (17), 4667–4672.

Li, K., Gao, X.-L., Wang, J., 2007. Dynamic crushing behavior of honeycomb structures with irregular cell shapes and non-uniform cell wall thickness. Int. J. Solids Struct. - Int. J. Solids Struct. 44, 5003–5026.

Liang, X., Chernysh, I., Purohit, P.K., Weisel, J.W., 2017a. Phase transitions during compression and decompression of clots from platelet-poor plasma, platelet-rich plasma and whole blood. Acta Biomater. 60, 275–290.

Liang, X., Shin, J., Magagnosc, D., Jiang, Y., Jin Park, S., John Hart, A., Turner, K., Gianola, D.S., Purohit, P.K., 2017b. Compression and recovery of carbon nanotube forests described as a phase transition. Int. J. Solids Struct. 122–123, 196–209.

Lopatnikov, S.L., Gama, B.A., Haque, M., Krauthauser, C., Gillespie, J.W., 2004. High-velocity plate impact of metal foams. Int. J. Impact Eng. 30 (4), 421–445.

Miao, M., 2013. Yarn spun from carbon nanotube forests: Production, structure, properties and applications. Particuology 11 (4), 378–393, Nanoscale Particuology.

Mueller, J., Matlack, K.H., Shea, K., Daraio, C., 2019. Energy absorption properties of periodic and stochastic 3D lattice materials. Adv. Theory Simul. 2 (10), 1900081.

Niemczura, J., Ravi-Chandar, K., 2006. Dynamics of propagating phase boundaries in NiTi. J. Mech. Phys. Solids 54 (10), 2136–2161.

Ozdemir, Z., Hernandez-Nava, E., Tyas, A., Warren, J.A., Fay, S.D., Goodall, R., Todd, I., Askes, H., 2016. Energy absorption in lattice structures in dynamics: Experiments. Int. J. Impact Eng. 89, 49–61.

Park, S.J., Shin, J., Magagnosc, D., Kim, S., Cao, C., Turner, K., Purohit, P., Gianola, D., Hart, A.J., 2020. Strong, ultralight nanofoams with extreme recovery and dissipation by manipulation of internal adhesive contacts. ACS Nano XXXX.

Pathak, S., Lim, E.J., Pour Shahid Saeed Abadi, P., Graham, S., Cola, B.A., Greer, J.R., 2012. Higher recovery and better energy dissipation at faster strain rates in carbon nanotube bundles: An in-situ study. ACS Nano 6 (3), 2189–2197, PMID: 22332591.

Peng, B., Locascio, M., Zapol, P., Li, S., Mielke, S., Schatz, G., Horacio, D., 2008. Measurements of near-ultimate strength for multiwalled carbon nanotubes and irradiation-induced crosslinking improvements. Nature Nanotechnol. 3, 626–631.
Petel, O.E., Ouellet, S., Frost, D.L., Higgins, A.J., 2014. Shock hugoniot measurements in foam. J. Phys. Conf. Ser. 500 (11), 112050.
Picu, C., Ganghoffer, J.-F., 2019. Mechanics of Fibrous Materials and Applications: Physical and Modeling Aspects, Vol. 596. Springer.
Portela, C.M., Edwards, B.W., Veysset, D., Sun, Y., Nelson, K.A., Kochmann, D.M., Greer, J.R., 2021. Supersonic impact resilience of nanoarchitected carbon. Nature Mater. 20 (11), 1491–1497.
Purohit, P.K., Bhattacharya, K., 2002. On beams made of a phase-transforming material. Int. J. Solids Struct. 39 (13), 3907–3929.
Purohit, P.K., Bhattacharya, K., 2003. Dynamics of strings made of phase-transforming materials. J. Mech. Phys. Solids 51 (3), 393–424.
Purohit, P.K., Litvinov, R.I., Brown, A.E., Discher, D.E., Weisel, J.W., 2011. Protein unfolding accounts for the unusual mechanical behavior of fibrin networks. Acta Biomater. 7 (6), 2374–2383.
Qi, C., Jiang, F., Yang, S., 2021. Advanced honeycomb designs for improving mechanical properties: A review. Composites B 227, 109393.
Raj, S., 2011. Microstructural characterization of metal foams: An examination of the applicability of the theoretical models for modeling foams. Mater. Sci. Eng. A 528 (15), 5289–5295.
Reid, S., Peng, C., 1997. Dynamic uniaxial crushing of wood. Int. J. Impact Eng. 19 (5), 531–570.
Rice, J.R., 1968. A path independent integral and the approximate analysis of strain concentration by notches and cracks. J. Appl. Mech. 35 (2), 379–386.
Ruzzene, M., Scarpa, F., Soranna, F., 2003. Wave beaming effects in two-dimensional cellular structures. Smart Mater. Struct. 12 (3), 363.
Schaedler, T.A., Jacobsen, A.J., Torrents, A., Sorensen, A.E., Lian, J., Greer, J.R., Valdevit, L., Carter, W.B., 2011. Ultralight metallic microlattices. Science 334 (6058), 962–965.
Shima, H., 2011. Buckling of carbon nanotubes: A state of the art review. Materials 5.
Smith, M.C., Cantwell, W., Guan, Z., Tsopanos, S., Theobald, M., Nurick, G.N., Langdon, G., 2011. The quasi-static and blast response of steel lattice structures. J. Sandwich Struct. Mater. 13, 479–501.
Sun, Y., Li, Q., 2018. Dynamic compressive behaviour of cellular materials: A review of phenomenon, mechanism and modelling. Int. J. Impact Eng. 112, 74–115.
Tan, P., Reid, S., Harrigan, J., Zou, Z., Li, S., 2005a. Dynamic compressive strength properties of aluminium foams. Part I—experimental data and observations. J. Mech. Phys. Solids 53 (10), 2174–2205.
Tan, P., Reid, S., Harrigan, J., Zou, Z., Li, S., 2005b. Dynamic compressive strength properties of aluminium foams. Part II—'shock' theory and comparison with experimental data and numerical models. J. Mech. Phys. Solids 53 (10), 2206–2230.
Tawfick, S., O'Brien, K., Hart, A.J., 2009. Flexible high-conductivity carbon-nanotube interconnects made by rolling and printing. Small 5 (21), 2467–2473.
Wang, P., Casadei, F., Kang, S.H., Bertoldi, K., 2015. Locally resonant band gaps in periodic beam lattices by tuning connectivity. Phys. Rev. B 91, 020103.
Wei, X., Li, D., Xiong, J., 2019. Fabrication and mechanical behaviors of an all-composite sandwich structure with a hexagon honeycomb core based on the tailor-folding approach. Compos. Sci. Technol. 184, 107878.
Winfree, N.A., 1999. Impact-Induced Phase Transformations in Elastic Solids: A Continuum Study Including Numerical Simulations for GeO (2). California Institute of Technology.
Xiong, J., Vaziri, A., Ghosh, R., Hu, H., Ma, L., Wu, L., 2016. Compression behavior and energy absorption of carbon fiber reinforced composite sandwich panels made of three-dimensional honeycomb grid cores. Extreme Mech. Lett. 7, 114–120, Mechanics in Extreme Manufacturing.
Yu, C., Shi, L., Yao, Z., Li, D., Majumdar, A., 2005. Thermal conductance and thermopower of an individual single-wall carbon nanotube. Nano Lett. 5 (9), 1842–1846.
Zhao, Q., Purohit, P.K., 2016. (Adiabatic) phase boundaries in a bistable chain with twist and stretch. J. Mech. Phys. Solids 92, 176–194.
Zheng, Z., Liu, Y., Yu, J., Reid, S.R., 2012. Dynamic crushing of cellular materials: Continuum-based wave models for the transitional and shock modes. Int. J. Impact Eng. 42, 66–79.
Zheng, Z., Wang, C., Yu, J., Reid, S.R., Harrigan, J.J., 2014. Dynamic stress–strain states for metal foams using a 3D cellular model. J. Mech. Phys. Solids 72, 93–114.
Zheng, Z., Yu, J., Li, J., 2005. Dynamic crushing of 2D cellular structures: A finite element study. Int. J. Impact Eng. 32 (1–4), 650–664.